Author Manuscript

Author Manuscript

Author Manuscript

Author Manuscript

HHS Public Access

Author manuscript

Cell Rep. Author manuscript; available in PMC 2026 March 04.

Published in final edited form as:

Cell Rep. 2025 October 28; 44(10): 116238. doi:10.1016/j.celrep.2025.116238.

Radiofrequency regulates the BET-mediated pathways in radial glia differentiation in human cortical development

Bilal Cakir[1], **Yoshiaki Tanaka**[1,7], **Mu Seog Choe**[1], **Ferdi Ridvan Kiral**[1], **Jonghun Kim**[1], **Nicola Micali**[2], **Young-Jin Kang**[3], **Bhushan Dharmadhikari**[4], **Benjamin Patterson**[1], **Woo Sub Yang**[1], **Yoonmi Cho**[1], **Yangfei Xiang**[1,8], **Mei Zhong**[5], **Sang-Hun Lee**[3], **Prabir Patra**[6,9], **Pasko Rakic**[2], **In-Hyun Park**[1,10,*]

[1]Department of Genetics, Yale Stem Cell Center, Wu Tsai Institute, Child Study Center, Yale School of Medicine, New Haven, CT 06520, USA

[2]Department of Neuroscience, Yale School of Medicine, New Haven, CT 06520, USA

[3]Department of Biomedical Sciences, Colorado State University, Fort Collins, CO 80523, USA

[4]Department of Electrical and Computer Engineering and Technology, Minnesota State University, Mankato, MN 56001, USA

[5]Department of Cell Biology, Yale Stem Cell Center, Yale School of Medicine, New Haven, CT, USA

[6]Department of Biomedical Engineering, and Department of Mechanical Engineering, University of Bridgeport, Bridgeport, CT 06604, USA

[7]Present address: Maisonneuve-Rosemont Hospital Research Center, Department of Medicine, University of Montreal, Montreal, QC H1T 2M4, Canada

[8]Present address: School of Life Science and Technology, ShanghaiTech University, Shanghai 201210, China

[9]Present address: Department of Biomedical Engineering, Marshall University, Huntington, WV, USA

[10]Lead contact

SUMMARY

The human brain represents one of the most complex organs in our body, with development regulated by an intricate genetic program. Recently, non-genetic factors, such as prenatal stress, infection, and diet, have been shown to influence brain development. Radiofrequency radiation

This is an open access article under the CC BY-NC-ND license (http://creativecommons.org/licenses/by-nc-nd/4.0/).

*Correspondence: inhyun.park@yale.edu.

AUTHOR CONTRIBUTIONS B.C. and I.-H.P. conceived the study. B.C., Y.T., M.S.C., J.K., F.R.K., N.M., Y.-J.K., and S.-H.L. performed the experiments. Y.-J.K. performed patch-clamp analyses. N.M. performed monkey primary cell isolation and culture. J.K. and F.R.K. performed immunofluorescence analyses. Y.T. analyzed single-cell sequencing data. P.P. and B.D. assembled the RF setup using transceiver modules. P.R. and I.-H.P. directed the research. B.C. and I.-H.P. wrote the manuscript. All authors read and commented on the manuscript.

DECLARATION OF INTERESTS

The authors declare no competing interests.

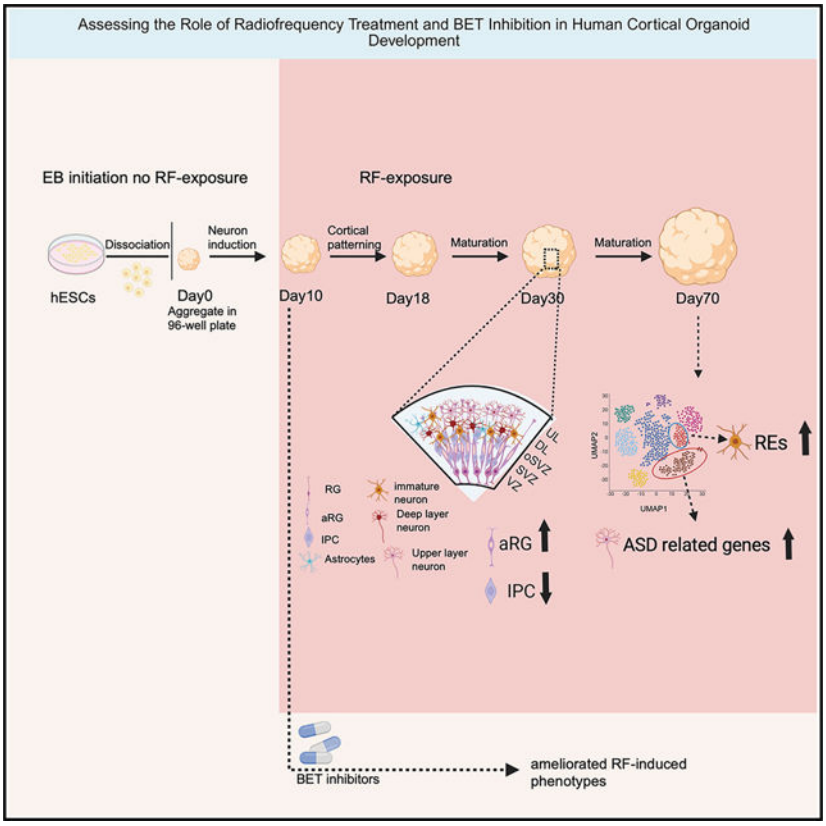
Author Manuscript Author Manuscript Author Manuscript Author Manuscript

(RF; 800–2,400 MHz), emitted by natural and artificial sources such as microwaves and cell phones, represents a non-invasive environmental factor. Using human cortical organoids (hCOs) derived from human embryonic stem cells (hESCs), we investigate RF's effects on corticogenesis. We find that RF exposure regulates the differentiation of human and non-human primate radial glia progenitors, maintaining stem cell identity and delaying differentiation. Neurons differentiated under RF treatment show induction of expression of human endogenous retroviruses. Importantly, inhibitors for the BET (bromodomain and extraterminal) protein rescue RF-induced developmental defects in hCOs. Our findings reveal a mechanism by which RF modulates early brain development, offering a non-biological approach to regulate neural stem cell self-renewal.

In brief

Cakir et al. show that radiofrequency exposure disrupts radial glial differentiation and induces autism-related gene expression in human cortical organoids. BET protein dysregulation underlies these effects, and BET inhibitors rescue the developmental defects.

Graphical Abstract



INTRODUCTION

Human cortical development is regulated by a series of steps that accompany neuroectoderm formation, neural tube formation, and cortical laminar layer formation. [1] Extensive research

Author Manuscript Author Manuscript Author Manuscript Author Manuscript

on the genetic regulation of cortical development over the years has uncovered several fundamental principles underlying human cortical development. Intriguingly, human genetic studies have identified mutations at critical genes for cortical development. [2] A large number of genes are known to be associated with neurodevelopmental disorders, such as autism spectrum disorder (ASD), intellectual disability, learning disorders, or neuropsychiatric disorders. [3–5]

In addition to the genetic regulation of human brain development, non-genetic factors play critical roles in the progression of human ectoderm commitment, neural tube formation, neural stem cell regulation, and neural maturation. Specifically, hormonal changes, drug treatment, or infection during pregnancy have shown a direct impact on fetal development, such as abnormal body development, brain development, and neuropsychiatric impact. [6] Recent studies have increasingly focused on the effects of environmental factors on neurodevelopment, highlighting the critical interplay between genetics and the environment in shaping brain architecture and function. [7] The electromagnetic field presents non-biological and non-invasive effects on the developmental program. While an electromagnetic field with a higher frequency and high energy can destroy biological materials, such as DNA, leading to cell death or mutations, radiofrequency radiation (RF) at a frequency of 800–2,400 MHz is commonly encountered in daily life. This RF is generated naturally by sources such as the sun and lightning, as well as artificially by household electronics like microwaves, Wi-Fi routers, and mobile phones. [8]

Recent studies have revealed the physiological impact of RF on biological systems, including oxidative stress, cell proliferation, and viability. [9] Several studies have shown that RF increases the proliferation of neural progenitor cells (NPCs). Murine NPCs and immortalized human neuroblastoma cell lines that are exposed to RF show an increase in proliferation and a concomitant decrease in differentiation. [10] However, it is still elusive how RF regulates human early NPC self-renewal and differentiation in the embryonic brain. Emerging evidence suggests that RF may impact the expression of key genes involved in neurodevelopmental processes, potentially affecting neurogenesis and the risk of neurodevelopmental disorders. For instance, a study by Eghlidospour et al. emphasizes the need for further investigation into how RF exposure alters differentiation pathways in neural stem cells, particularly in relation to apoptosis and cell cycle regulation. Other studies have indicated that electromagnetic field (EMF) exposure may induce stress responses in stem cells, affecting their development and function.

In recent years, the advent of human cortical organoids (hCOs) has revolutionized the study of brain development by providing models that more accurately reflect human physiology compared to traditional 2D cell cultures. [11,12] These organoids exhibit complex 3D architectures and cellular diversity, allowing researchers to explore cellular interactions and developmental processes in ways that previous models, focusing on animal models or simple neural stem cell cultures, could not. [11,13,14] By utilizing hCOs derived from human embryonic stem cells (hESCs), our research provides a more physiologically relevant context in which to investigate the effects of RF exposure on cortical neural stem cells, bridging the gap between *in vitro* findings and *in vivo* conditions.

Author Manuscript Author Manuscript Author Manuscript Author Manuscript

Here, we set out to use hCOs as a model system to elucidate how RF regulates the self-renewal of human cortical neural stem cells. Our study offers several important contributions to the understanding of how RF influences early neural development using hCOs. Unlike previous studies that primarily relied on animal models or immortalized cell lines, our research utilizes hCOs derived from hESCs, providing a more physiologically relevant and human-specific context for investigating the effects of RF on cortical neural stem cells.

RESULTS

RF increases the proliferation of radial glia in hCOs

To investigate the effect of radiofrequency on human cortical development, we constructed a device that generates a uniform RF field (Figure S1A). As a model for the developing early human brain, we generated hCOs from hESCs and exposed them to 12 or 24 h/day RF cycles throughout their development, beginning from the patterning stage at day 10 (Figure 1A). [15,16] Following the 12 h/day exposure, hCOs showed an irregular surface shape from post-exposure day 8 (Figure S1B), but no significant change in the overall size was observed (Figure S1C). 24 h/day RF treatment caused a considerable reduction in size (Figure 1B). However, after 2 months in culture under RF exposure, hCOs recovered from the abnormal morphology and the smaller size observed at an early stage (Figure 1B). Overall, these results suggest that RF affects brain organoid development at an early stage of development.

The developmental program of hCOs recapitulates the phases and features of human corticogenesis. These include the formation of apical radial glial cells (aRGs) that arise at the germinal ventricular-like zone (VZ) and subventricular-like zone (SVZ) and differentiate into glutamatergic excitatory neurons. [11,17–20] The reduction in the size of hCOs by RF treatment at the early developmental stage suggests that aRG self-renewal or differentiation is regulated by RF (Figure 1B). To test this hypothesis, we examined the mitotic behaviors of SOX2+ aRGs by measuring the angle of the orientation relative to the apical surface of hCOs. [15] Immunostaining for phospho-histone H3 indicated that RF dramatically increased in aRGs with vertical cleavage compared to control hCOs (Figure 1C). As the vertical cleavage represents self-renewal of aRGs, RF-treated organoids showed an increase in SOX2+ aRGs at both early and mid-stages of development (Figures 1C–1E and S1D). We further assessed the effects of RF on TBR2+ intermediate progenitors and CTIP2+ deep-layer subcortical neuronal differentiation. [21] Consistent with the reduced organoid size and mitotic behaviors of aRGs during the early stage of cortical development, we found a significant decrease in TBR2+ intermediate progenitors and CTIP2+ deep-layer neurons in the RF-treated organoids (Figure 1E). Interestingly, RF-treated hCOs exhibit increased SOX2+ aRGs and decreased CTIP2+ neurons at both early- and mid-stage organoid development (Figures 1F and S1D). Birth dating of newborn cells using 5-ethynyl-2′-deoxyuridine (EdU) pulse-chase labeling for 7 days confirmed the sustained production of SOX2+ RG cells under RF treatment (Figure 1G). Additionally, an overall increase in phospho-histone $H3^+$ cells within the VZ, along with a higher ratio of EdU-labeled cells inside versus outside the VZ, suggests that RF exposure promotes the expansion of aRGs at the expense of intermediate progenitors and deep-layer neurons (Figures S1E and S1F).

Author Manuscript Author Manuscript Author Manuscript Author Manuscript

Together, these results indicate that RF exposure enhances aRG self-renewal by increasing symmetric (vertical) cell divisions, thereby altering early corticogenesis.

To further validate the effect of RF on non-human primate mid-fetal RGs, we isolated the primary neural stem cells from the fetal rhesus macaque cortex (rNSCs) at embryonic day (E)54 and cultured them in a high FGF2 condition (20 ng/mL) that supports NSC proliferation, as previously established. [16] RF treatment of proliferating rNSCs for 6 days (day *in vitro* [DIV]6) increased the expression of the neural stem cell marker SOX2 but decreased the neuronal gene TUJ1 (Figures S2A and S2B), consistent with the hCOs exposed to RF. We further tested the RF treatment on differentiating rNSCs,[16] which was induced by culturing them in low-FGF2 (1 ng/mL) conditions. RF treatment decreased the neuronal differentiation marked by reduced TUJ1, MAP2, and SATB2 levels at DIV22 while increasing rNSC proliferation as marked by increased SOX2 expression (Figures S2B and S2C). Overall, these results further support that RF induces NSC proliferation but inhibits differentiation during primate cortical development.

RF treatment leads to dysregulated gene expression program

To decipher how RF regulates neurodevelopmental processes, we performed single-cell RNA sequencing (scRNA-seq) on RF-treated and non-treated hCOs at day 70 (Figure 2A). The electromagnetic shield blocks RF exposure, and aluminum foil also offers partial protection. [22] Thus, we also performed scRNA-seq on hCOs covered by a shield or aluminum foil and treated with RF. A total of 31,094 cells were profiled and systematically assigned into 13 cell types (25 clusters) using canonical markers for each cell type (Figures 2B and S3A–S3C). [23] A dramatic downregulation of genes involved in RNA processing, translation, and cellular metabolism was found in hCOs treated with RF (Figure 2C). Moreover, the RF increased the expression of genes associated with neurodevelopment and neuronal projection (Figure 2C). Interestingly, the differentially expressed genes by RF treatment were attenuated with the shield but only partially attenuated with the aluminum foil. These results suggest that early human brain development is regulated by a biological program affected by RF.

To investigate whether RF treatment is related to the expression of neural disease-related genes, we performed gene set enrichment analysis (GSEA) of DisGeNet genes (Figure S3D). [24] We found that ASD-related genes displayed more significant differential expression between RF-treated and non-treated hCOs than other neurological diseases. RF-treated hCOs without shield protection showed a higher expression of ASD-related genes (Figure S3D, false discovery rate [FDR] = 0.037). The shield almost entirely protected from the induction of the ASD genes, but aluminum foil was only partly effective (Figure S3D). To further dissect RF-mediated regulation of ASD genes, we analyzed the overrepresentation of 393 high-confidence risk genes from the SFARI (Simons Foundation Autism Research Initiative) database across cell types or clusters (Figures 2D and S3E). [25] GSEA revealed a significantly higher expression of SFARI genes in RF-treated hCOs, and the aluminum foil was not protective (FDR < 0.05). In particular, RF-mediated induction of SFARI genes, including NSD1, SCN2A, AUTS2, TBR1, and FOXG1, was detected in neuronal clusters (cortical neuron [CN], interneuron [IN], neuron, and inter), a neuronal progenitor

Author Manuscript Author Manuscript Author Manuscript Author Manuscript

cluster (NPC), and a part of glial clusters (glial progenitor cells [GPCs] and radial glial cells [RGCs]) (Figure 2E). RT-qPCR confirmed the findings from scRNA-seq data and showed an elevated expression of ASD-related genes (e.g., NSD1, ARX, FOXG1, NCOA1, CPEB4, and TBR1) in RF-treated hCOs compared to control hCOs at day 70 (Figure 2F). Immunostaining further confirmed the elevated expression of FOXG1, AUTS2, and CPEB4 proteins in hCOs with RF treatment (Figures 2G and 2H). Notably, CPEB4 is known to regulate mRNA translation, whose dysregulation is directly associated with ASD. [26] Indeed, RF-treated organoids demonstrated Gene Ontology (GO) terms related to impaired translation (Figure 2C). Despite the significant changes in ASD-related gene expression, non-SFARI neurodevelopmental genes did not show a clear difference between RF-treated and non-treated hCOs (Figure S3F), suggesting that the differential expression of ASD-related genes is not caused by global neuronal program dysregulations. Overall, RF-treated organoids (day 70) exhibit the gene expression programs associated with ASD, which the shield can protect.

Patients with neurodevelopmental disorders, including ASD, exhibit aberrant overexpression of a part of a retrotransposable element (RE) in the brain.[27,28] Mapping of scRNA-seq reads to RE transcripts revealed that RE-derived unique molecular identifier (UMI) reads significantly increased in RF-treated hCOs (Figure S4A), suggesting that RF exposure induces RE expression. In addition, the shield and aluminum fold significantly reduced the RF-mediated RE induction (Figure S4A). We also found that RE expression is dramatically higher in one immature neuronal cluster (labeled as ‘‘neuron4’’) that expresses axonal growth genes (e.g., STMN2, GAP43, and DCX) but lacks neurotransmitter transporters (e.g., vGLUT1/2 and vGAT) ($p < 2.2e{-}16$ by two-sided t test) (Figure S4B). In this neuronal cluster, RF exposure led to the induction of several REs, such as SVA (SINE-VNTR-Alu), LINE (long interspersed nuclear element), and long terminal repeat (LTR) (Figure S4C). Like ASD risk genes, RF-induced RE expression was reduced by the shield but not by aluminum foil. We confirmed the findings using RT-qPCR, which showed the overexpression of REs, particularly L1PA16, L2a, L1ME4a, and THE1A, in RF-treated hCOs (Figure S4D). Upregulation of REs (L1PA16, L2A), as well as other ASD-related genes (SCN2A1, NSD1, THE1A), was also observed in RF-treated primary monkey NSCs and the derived neurons (Figure S4E). Collectively, these results indicate that RF exposure promotes the aberrant expression of ASD risk genes as well as REs.

Functional defects in RF-treated neurons

To examine how RF regulates the development and function of cortical neurons, we labeled neurons with an adeno-associated virus (AAV) driving enhanced (E)GFP expression under a human synapsin promoter. RF treatment leads to a significant increase in dendritic spine density compared to neurons from control hCOs (Figure 3A). Consistently, co-staining for the neuronal marker MAP2 and the synaptic marker PSD95 revealed a significantly higher number of synapses in RF-treated organoids relative to controls (Figure S4F). We next investigated the functional consequences of RF exposure in brain organoids by utilizing the genetically encoded GCAMP6s. [15] In hCOs, neurons displayed spontaneous calcium transients (Figure 3B; Video S1). On the other hand, neurons from RF-treated organoids showed more neuronal activity with enhanced intensity (Figure 3B; Video S1). Thus, our

Author Manuscript Author Manuscript Author Manuscript Author Manuscript

data suggest that RF exposure leads to altered neuronal functions exhibiting upregulated neuronal activity. We further performed whole-cell patch-clamp recordings in RF-treated hCOs and control hCOs (Figure 3C). A larger portion of cortical cells from RF-treated hCOs produced action potentials in response to 1-s depolarizing current steps (from +5 to +20 pA) compared to the portion from control hCOs (Figure 3D; RF treated: 8 cells showing APs/16 tested cells; control: 1 cell showing APs/14 tested cells; $p = 0.0169$, Fisher's exact test). Next, we examined whether neurons from RF-treated hCOs show major changes in other intrinsic biophysical properties. There was no significant difference in resting membrane potentials (V_{rest}) between neurons from RF-treated hCOs and control hCOs (Figure 3E; RF treated: −46.8 ± 5.5 mV, $n = 12$; control: −55.9 ± 6.2 mV, $n = 9$; $p = 0.214$, Mann-Whitney [MW] U test). In addition, neurons from RF-treated hCOs showed similar input resistance (R_{input}) and membrane time constant ($\tau_{membrane}$) to those of neurons from control hCOs (Figures 3F–3H; R_{input} : RF treated, 2.2 ± 0.3 GΩ, $n = 15$; control, 2.5 ± 0.5 GΩ, $n = 12$; $p = 0.864$, MW U test; $\tau_{membrane}$: RF treated, 72.2 ± 14.1 ms, $n = 15$; control, 75.1 ± 17.6 ms, $n = 12$; $p = 0.864$, MW U test). The results suggest that RF treatment increases neuronal activity in hCOs but does not cause major changes in other intrinsic properties of neurons.

Pharmacological rescue of RF-induced damage in hCOs

In our previous studies on Rett syndrome with MeCP2 mutations, hCOs with MeCP2 mutated at arginine 133 to cysteine (R133C) displayed a developmental delay in neural maturation. [29] We have integrated and compared scRNA-seq data from R133C hCO and RF-treated hCO data (Figures 4A, S5A, and S5B). Interestingly, R133C hCOs showed the same increase in the NPC population as RF-treated hCOs (Figure 4B). Furthermore, pseudotime analysis revealed that RF-treated hCOs display an increase in the number of cells at early pseudotime as observed in R133C hCOs, indicating developmentally delayed populations (Figure 4C). Furthermore, differentially expressed genes in RF-treated hCOs show significant overlap with R133C hCOs, including FOXG1, EMX1, TBR1, and FEZF2 (Figures 4D and 4E). High expression of HES1, a critical transcription regulator for NPC proliferation (Figure 4F), in RF-treated hCOs and R133C hCOs implicates the continued activation of NOTCH signaling in both RF and R133C hCO development.

Based on the fact that R133C hCOs and RF-treated hCOs share similar phenotypes, we hypothesized that JQ1 or related inhibitors for the bromodomain and extraterminal (BET) protein that recovered the phenotypes in R133C hCOs could rescue the phenotypes in RF-treated hCOs. Recent studies have shown that BET inhibition can recover phenotypes associated with MeCP2 mutations that lead to dysregulated neural maturation. [29] Given the developmental delays observed in both R133C and RF-treated organoids, it is plausible that BET proteins may also be altered in RF-treated hCOs. We propose that BET proteins could be downregulated in RF-treated organoids, and their inhibition might provide therapeutic benefits by rescuing the delayed differentiation seen in these organoids. Notably, two BET inhibitors (JQ1 and iBET762, 50 nM) rescued the RF-driven morphological change and the reduced size of hCOs at early organoid development (Figure 5A). In addition, we examined the effects of these inhibitors on RF-induced ASD-associated gene transcription at a later stage of hCO development. When treated with iBET762 or JQ1, RF-treated hCOs showed a decrease in expression of ASD-associated genes (TBR1, ARX, FOXG1, SOX5, CPEB4,

Author Manuscript Author Manuscript Author Manuscript Author Manuscript

NCOA1, NSD1, and SCN2A) and REs (L1PA16, L2a, L1ME4a, and THE1A) (Figures 5B and 5C). Moreover, iBET762 treatment restored neuronal differentiation markers and proliferation dynamics: it rescued CTIP2 expression, normalized EdU incorporation and phospho-histone $H3^+$ mitotic activity in $SOX2^+$ radial glia (Figures 1G, S1E, and S1F), and reversed the excessive synapse formation observed in RF-treated organoids (Figure S4F). These results suggest that RF regulates early human cortical development via histone acetylation-mediated epigenetic pathways.

To investigate the mechanism behind the RF-induced phenotype changes, we performed scATAC-seq analysis in three conditions: non-treated, RF treated, and RF/iBET treated. We then integrated the scATAC-seq data with previously acquired scRNA-seq datasets, using gene activity scores to reconstruct cell clusters and confirm proper clustering via uniform manifold approximation and projection (UMAP) and other methods (Figures S6A and S6B). The open-chromatin area in RF-treated hCOs showed a selective and marked enrichment in GO terms related to early NPC development (Figure 6A). To identify the factors that directly regulate this increased NPC population, we performed a motif enrichment analysis on the promoter regions with the open-chromatin status and found a pronounced increase in TF binding motifs that potentially facilitate neuronal development under RF treatment (Figure 6B). Notably, the binding motif for NRF1, a well-known transcription regulator in neural development, exhibited substantial enrichment, showing a co-expression pattern with other histone modification-mediated epigenetic factors such as NSD3 and JMJD1C (Figures 6C and 6D). These findings suggest that these epigenetic regulators interact to modulate chromatin accessibility, regulating the neural maturation delay observed in RF treatment. When iBET was treated, the number of genes exhibiting altered chromatin accessibility under RF treatment made a dramatic decrease from 1,906 to 191, indicating a substantial restoration of chromatin accessibility status. This result is consistent with the reduction of the expanded NPC population under iBET treatment (Figure 6E). Altogether, our data found that iBET rescues the NPC maturation delay by RF-altered epigenetic regulators, suggesting the therapeutic potential of BET inhibition for restoring neurodevelopment in RF- or loss of function in ASD-related genes.

DISCUSSION

The human brain developmental program has been investigated with postmortem brain or primary fetal brain from an abortion. Overcoming the ethical issue of obtaining the research materials and the scarcity of tissue, human stem cell-derived hCOs, or other brain organoids has offered unlimited resources for brain tissue. [30] A large body of research using hCOs has elucidated the function of genes associated with neurodevelopmental and neuropsychiatric disorders. [29,31] Additionally, recent studies have started investigating the impact of non-genetic environmental factors on human brain development, including viral infection, substance, medicine, and stress. [32] These environmental factors are known to leave a long-lasting effect on brain function and even the behaviors of offspring. Infection by Zika and herpes simplex viruses causes a severe brain malformation, such as microcephaly, and hCOs turn out to be an excellent model to replicate viral infection-mediated microcephaly. [33] The effects of ethanol, nicotine, or cannabis on the development of cerebral organoids have been actively investigated. [34,35] Nicotine treatment in the early stage of cerebral

Author Manuscript Author Manuscript Author Manuscript Author Manuscript

organoids induced neural death in cerebral organoids, leading to an increase in TUJ1^{+} neurons, a hallmark of premature differentiation of NPCs. [35] When treated on more advanced cerebral organoids, nicotine caused an increase in CTIP2+ deeper-layer neurons while decreasing TBR1+ upper-layer neurons. Ethanol treatment has an impact on NPCs similar to nicotine treatment, causing neural death and premature differentiation. [35,36]

In our study, we observed a defect in cell fate characterized by delayed differentiation, raising questions about the implications of asymmetric versus symmetric divisions in cortical development. Apical-basal progenitor cell polarity is pivotal for establishing the radial and laminar architecture of the developing human cortex. [1] The diversity and expansion of cortical stem cell populations have been mirrored by increasingly complex cellular processes that regulate stem cell morphology and behavior. [37] Distinctive symmetric divisions of neuroepithelial cells are prominent in younger organoids, while older organoids show an increase in radial glial progenitors, which demonstrate a variety of cleavage angles and division types. [38,39] This balance between symmetric amplification and asymmetric neurogenic divisions influences the size of cortical organoids; despite producing the same number of cells, asymmetric divisions yield smaller organoids due to a reduced pool of proliferative progenitor cells. This dynamic is critical for understanding how cortical architecture is affected by environmental factors, such as RF exposure.

No major neurodevelopmental defect has been linked with RF exposure, mainly due to its relatively weak energy compared with X-rays or gamma rays. [40] However, emerging evidence suggests that prolonged RF exposure may have subtle neurodevelopmental implications. Recent studies in animal models exposed chronically to RF have shown autism-like behaviors, raising concerns about the impact of RF on neurodevelopment. [41] For instance, behavioral changes such as hyperactivity and cognitive deficits observed in animal models highlight the need for further exploration into the neurodevelopmental consequences of RF exposure in humans. Although decades' worth of studies have reported a broad range of adverse impacts from RF on human health, RF-mediated dysregulation of human brain development has remained largely unknown. In this study, we showed the detrimental effects of RF exposure to cortical organoids. [42]

The perinatal period in neurogenesis encloses a distinctive window embodying diverse molecular and cellular processes required for proper development. [5] Though prenatal brain development comprises high plasticity, it is vulnerable to internal and external perturbations. Thus, environmental insults, including chemicals, drugs, pollution, stress, and even prolonged ultrasound wave exposure, can permanently impact brain development and subsequent behavior. [43,44] Our findings revealed that RF-exposed cortical neurons exhibited increases in ASD-associated gene expression and dendritic spine density, characteristics of patients on the autism spectrum. [45] Furthermore, the parallels drawn from *in utero* RF exposure in animal models, which have demonstrated behavioral changes such as hyperactivity and memory deficits, underscore the relevance of our findings in a human context. [41,46] These findings suggest a potential shared mechanism by which RF exposure may contribute to neurodevelopmental disorders across species. Altered morphology and transcriptome driven by RF exposure in hCOs further lead to aberrant and enhanced neuron firing. In fact, *in utero* RF exposure in mice models results in behavioral and cognitive

Author Manuscript Author Manuscript Author Manuscript Author Manuscript

changes such as hyperactivity and memory deficit. [41] Notably, we showed that physical barrier protection or chemical treatment could attenuate the RF-induced damage during cortical organoid development.

Here, we have thoroughly examined the effects of RF exposure and demonstrated RF-induced changes associated with ASD in the transcriptomics, morphology, and function of cortical neurons. This addition to the literature is particularly significant given that most studies have historically focused on genetic causes of ASD, while environmental factors, particularly RF exposure, have been understudied. By utilizing induced pluripotent stem cell (iPSC)-derived hCOs, our research offers insights that bridge the gap between animal models and human neurodevelopment. The use of human organoids enables us to detail the specific impacts of RF exposure on human neuronal cells, which may differ from findings observed in animal models.

Our findings also point to the potential involvement of BET proteins in the regulation of neurodevelopmental pathways affected by RF treatment. We propose that BET proteins may be altered in RF-treated hCOs, similar to how they are affected in Rett syndrome model organoids with MeCP2 mutations. [29] It remains to be determined whether BET proteins are significantly downregulated in RF-treated organoids. If so, the inhibition of BET proteins could serve as a therapeutic strategy to rescue delayed differentiation in these organoids. This interaction raises the question of whether RF exposure and BET regulation function in an epistatic relationship or operate independently.

Limitations of the study

Despite these significant findings, there are notable limitations to our study. Our model lacks physical barriers, such as the amniotic sac and the immature skull, which begins to form around the fourth week of gestation. [47] This limitation is particularly relevant, as it may influence the vulnerability of neural tissue to environmental insults, including RF exposure. Future studies could incorporate synthetic bone-like structures to evaluate their potential protective effects on neural tissue against RF exposure. Additionally, the genetic homogeneity of the stem cell lines used to generate organoids may not accurately reflect the genetic diversity present in the broader human population or in specific neurodevelopmental disorders, which may limit the generalizability of our results. [48] The temporal constraints of organoid development further complicate the capture of the long-term processes inherent in human brain development, particularly regarding chronic RF exposure. [49] To strengthen our understanding, it would be beneficial to integrate complementary models, such as *in vivo* studies or genetically diverse organoid systems, to validate our observations. Longitudinal studies assessing the sustained impacts of RF exposure and the incorporation of immune cells—whose role in RF-induced inflammation is notably absent in our current hCO model [50] —could yield valuable insights. [11,51] Moreover, while this study focuses on cortical organoids that model the development of glutamatergic excitatory neurons, it remains critical to investigate how RF treatment affects other neuronal populations, such as GABAergic inhibitory neurons derived from the ventral telencephalon or non-cortical neurons, through the use of region-specific brain organoids. [15,52]

Author Manuscript Author Manuscript Author Manuscript Author Manuscript

Thus, employing region-specific brain organoids could enhance our understanding of the contributions of environmental insults to fetal brain development. Finally, discussing the broader implications of these findings in the context of public health and policy is crucial given the ongoing debates surrounding RF exposure and its potential risks.[53] Addressing these points will enrich our comprehension of the multifaceted nature of neurodevelopment and the impact of environmental factors on brain health.

RESOURCE AVAILABILITY

Lead contact

Further information and requests for reagents may be directed to, and will be fulfilled by the lead contact, Dr. In-Hyun Park (inhyun.park@yale.edu).

Materials availability

Materials generated in this study are available from the lead contact upon request, subject to a completed materials transfer agreement.

Data and code availability

- The accession number of the data generated in this study is GEO: GSE302899, which is listed in the key resources table.
- This paper does not report original code.
- Any additional information required to reanalyze the data reported in this paper is available from the lead contact upon request.

STAR★METHODS

EXPERIMENTAL MODEL AND STUDY PARTICIPANT DETAILS

hESCs culture: HES-3 NKX2–1GFP/w, and H1 hESCs were cultured on Matrigel (BD Biosciences) coated cell culture dishes with mTeSR1 media (Stem Cell Technologies). hESCs were confirmed pluripotent and mycoplasma free, and were passaged every week by treatment with Dispase (0.83 U/ml, Stem Cell Technologies). All experiments including hESCs were approved by Yale Embryonic Stem Cell Research Oversight (ESCRO).

Animals: All animal experiments were approved by the Institutional Animal Care & Use Committee (IACUC) of the Yale University.

Generation of cortical organoids (hCOs): As we described earlier, [14] 9000 cells were plated into a well of U-bottom ultra-low-attachment 96-well plate in neural induction media (DMEM-F12, 15% (v/v) KSR, 5% (v/v) heat-inactivated FBS (Life Technologies),1% (v/v) Glutamax, 1% (v/v) MEM-NEAA, 100 μM β-Mercaptoethanol) supplemented with 10 μM SB-431542, 100 nM LDN-193189, 2 μM XAV-939 and 50 μM Y27632. FBS and Y27632 were removed from day 2 and 4, respectively. The media was replenished every other day until day 10, where organoids were transferred to ultra-low-attachment 6-well plate. The organoids were cultured in spinning hCO media with minus vitamin A

Author Manuscript Author Manuscript Author Manuscript Author Manuscript

(1:1 mixture of DMEM-F12 and Neurobasal media, 0.5% (v/v) N2 supplement, 1% (v/v) B27 supplement without vitamin A, 0.5% (v/v) MEM-NEAA, 1% (v/v) Glutamax, 50 μM β-Mercaptoethanol, 1% (v/v) Penicillin/Streptomycin and 0.025% Insulin). The media was replenished every other day until day 18, where media was switched to the hCO media with vitamin A (the same composition as described above except B27 with vitamin A) supplemented with 20 ng/mL BDNF and 200 μM ascorbic acid. The media was changed every 4 days after day 18.

NSC isolation and differentiation: All animal procedures were performed in accordance with the policies of the Yale Institutional Animal Care and Use Committee. Rhesus macaque monkeys were bred in Rakic primate breeding colony at Yale and timed pregnant females underwent caesarian section at the required embryonic age. E54 fetal rhesus macaque cortices were collected and dissected. Then tissue was incubated with HBSS-Papain (2 mg/mL) (BrainBits)-DNase I 0.1mg/ml (StemCells) solution 25 min at 37 C. The solution was replaced with DMEM/F12 medium plus N2 supplement (below), and by mechanical trituration single cells were obtained. Cells were counted and plated onto 10 cm dish (Falcon 35–3003) previously coated with poly-L-ornithine (PLO) (Sigma, P3655) and fibronectin (FN) (R&D Systems, 1030FN), and incubated at 37 C, 5% O2, 5% CO2 in DMEM/F12 medium (Mediatech 16–405-CV) plus N2 supplement, containing 25 μg/mL bovine insulin (Sigma, I6634), 100 μg/mL apotransferrin (Sigma, T2036), 20 nM progesterone (Sigma, P8783), 100 μM putrescine (Sigma, P5780), 30 nM sodium selenite (Sigma, S5261), penicillin/streptomycin (Life technology, 15140–122), as previously described. [16] FGF2 (R&D Systems, 4114-TC) 20 ng/mL was added daily. Expanded cortical NSCs were then detached with Accutase at DIV6 and banked at −80C.[60,61]

Thawed E54 monkey NSCs were expanded in DMEM/F12 plus N2 supplement in presence of 20 ng/mL FGF2 for 5 days until confluence. NSCs were dissociated with Accutase (Life Technologies, A11105) and passage into PLO/fibronectin-coated 24 well plates (IBIDI, 82406), at a density of 250.000/well in DMEM/F12/N2 medium plus varying doses of FGF2 (1 or 20 ng/mL) for 6 days. FGF2 was added daily. Differentiation of NSCs was induced at DIV6 by FGF2 withdrawal. Cells were kept in DMEM/F12 plus N2 supplement. At DIV8, medium was replaced with NeuroBasal (NB) (Life technology, 12348–017), containing 25 μg/mL insulin, 30 nM sodium selenite, Glutamax (Life technology, 35050061), 1x B27 (Life Technologies, 17504–044), 10 ng/mL BDNF (R&D Systems, 248-BD) and 10 ng/mL NT-3 (R&D Systems, 267-N3) until DIV22. Cells were fixed with 4% PFA or RNA was extracted using RNAeasy kit (Quiagen) at DIV6 or DIV22.

METHOD DETAILS

RFID setup: Generation of the uniform RF field that can mimic the transceiver module of a smartphone was the necessary criteria. For this we have used the DSD TECH HC-05 Bluetooth Serial Pass-through Wireless Serial Communication module, which is programmed using Arduino Uno R3 Microcontroller A000066. Serial port Bluetooth module is fully qualified Bluetooth V2.0+EDR (Enhanced Data Rate) 3Mbps Modulation with complete 2.4GHz radio transceiver and baseband. The wireless serial communication

Author Manuscript Author Manuscript Author Manuscript Author Manuscript

module is designed to transmit and receive a simple string of 1's and 0's with a fixed baud rate of 38400. RF exposure was conducted using a DSD TECH HC-05 Bluetooth module, operating at a frequency of 2.4 GHz (Bluetooth V2.0+EDR) with a transmission output power of 4 dBm (2.4 mW), consistent with low-power Bluetooth devices. The organoids were placed 1 inch from the RF source to ensure consistent exposure. The estimated specific absorption rate (SAR) and power density at the exposure distance (1 inch) were measured using a standard RF meter—CORNET high-performance Electrosmog meter—with the maximum field strength recorded at 2.5 mW/m^2. The experimental setup was enclosed in an RF shield constructed from Faraday Copper Fabric-EMI RFID Copper (Amradield), measuring 0.5 mm in thickness [127 mm × 85 mm × 23 mm], achieving a shielding effectiveness of [80–115 dB (MIL-DTL-83528C)] to minimize external RF interference.

Control Conditions: The hCOs were cultured in separate incubators without intentional RF exposure. However, it is important to note that these control organoids may still be exposed to ambient RF levels present in the environment. While we implemented strategies to minimize exposure by situating the incubators away from high RF-emitting devices and monitoring environmental RF levels, complete shielding from all sources of RF cannot be guaranteed. This acknowledgment is crucial for interpreting our findings, as it recognizes the potential for background RF exposure in both control and experimental conditions.

Cryosectioning and immunostaining: As described earlier, [15] all hCOs were fixed in 4% paraformaldehyde (PFA) at 4° C overnight. After washing with PBS three times, they were incubated in 30% sucrose solution for 2 days at 4° C. Organoids were embedded in O.C.T in base molds on dry ice and sectioned for 40-μm. The organoid blocks were further stored at −80° C. After sections were dried, they were incubated with 0.3% Triton-100 for 15 min and further blocked with 3% bovine serum albumin (BSA) for 2 h at RT. Then, the primary antibody, diluted in 3% BSA, incubation is performed at 4° C overnight. After washing with PBS, organoids were incubated with Alexa Fluor dyes (1:1000) for 1 h and following nuclei staining with DAPI (1:1000) for 10 min at RT. Finally, slides were mounted with ProLong Gold Antifade Reagent and images were taken with Leica TCS SP8 confocal microscope.

Data processing of single-cell RNA sequencing (scRNA-seq): Assignment of scRNA-seq reads to hg19 human genome and counting in Ensembl genes were implemented by count function of CellRanger (v3.0.2) with default parameters. UMI count matrix from each library was harmonized by Seurat (v3.0.2). [55] First, cells with more than 500 genes and less than 20% mitochondria-derived reads and genes expressed in more than five cells were retained for subsequent analyses. Raw UMI count was then normalized to total UMI count. Cell pair anchoring was performed by top 2,000 highly variable genes with 20 dimensions of canonical correlation analysis. After scaling gene expression values across all integrated cells, dimensional reduction was implemented using principal component analysis (PCA). For visualization, Individual cells were projected into two-dimensional UMAP space using from 1st to 20th PCs. Graph-based clustering was performed with shared nearest neighbor method from 1st to 20th PCs and 0.8 resolution value. Differentially-expressed genes (DEGs) in each cluster were identified with more than 1.25-fold change and $p <$

Author Manuscript Author Manuscript Author Manuscript Author Manuscript

0.05 by two-sided unpaired T test. Gene Ontology analysis was performed to the DEGs by GOstats Bioconductor package (v2.46.0). False discovery rate was adjusted by p.adjust function in R with ‘‘method = ’’BH’’’’ parameter. To integrated scRNA-seq dataset with MeCP2 scRNA-seq dataset, MeCP2 scRNA-seq data from the Gene Expression Omnibus (GEO) (GSE117513) were used. For data integration, we first identified the top 2,000 highly variable genes (HVGs) in each scRNA-seq dataset and then used these HVGs in the FindIntegrationAnchors function to identify common cell pairs and estimate anchors. We performed principal component analysis (PCA) using 20 dimensions, and subsequently integrated the datasets at a consistent scale through the IntegrateData function using the identified anchors. Finally, we standardized (scaled) the gene expression values in the integrated dataset with ScaleData, performed PCA and UMAP reduction again.

Cell type in each cluster was determined with unique markers, Gene Ontology and the reference transcriptome of human brain cell types (Figures S3A and S3B).[23] First, we classified 12 neuronal and 12 non-neuronal clusters with expression of neuronal growth cone markers (STMN, GAP43 and DCX) and early neurogenesis markers (VIM, HES1 or SOX2), respectively. A cluster with the substantial expression of growth cone and early neurogenesis genes was assigned as ‘‘intermediate’’. The neuronal clusters were separated into cortical (CN) and interneuron clusters (IN) by glutamate transporters (SLC17A6 and SLC17A7) and GABA transporters/Glutamate decarboxylase (SLC32A1, GAD1 and GAD2), respectively. Neuronal cells without neurotransmitter transporters were labeled as ‘‘immature neuron’’.

Among non-neuronal clusters, seven clusters show significant enrichment of genes involved in ‘‘glial cell development (GO:0021782)’’ (FDR <0.05). Two glia cell clusters also showed higher expression of ‘‘astrocyte development (GO:0048708)’’ genes (FDR < 1e-3) and key astrocyte (AS) markers (e.g., SLC1A3 and GFAP). Two other glia cell clusters displayed substantial expression of outer radial glia markers (e.g., HOPX) and were assigned as radial glia cells (RGC). A glia cluster with ‘‘mitotic nuclear division (GO:0007067)’’ (FDR <0.05) was labeled as neuronal progenitor cells (NPCs). Two glia clusters without AS, RGC mitotic markers was defined as glia progenitor cell (GPC). For integrated scRNA-seq data, total of 28 clusters were defined based on the expression patterns of a custom marker gene set. Clusters expressing SLC17A6 were assigned as excitatory neurons (ExN). Clusters where DCX and MAP2 were present, but with low expression of GAD1 and SLC17A6, were labeled as general ‘‘neurons.’’ Clusters that showed high expression of GAD1 were classified as inhibitory neurons (InN). Radial glia cells (RGC) were identified by elevated expression of FABP7, and neuronal progenitor cells (NPCs) were characterized by PAX6, SOX2, and HES5. A cluster with strong LMX1A expression was assigned as the Hem, which was further subdivided into choroid plexus (ChP) if TTR and CLIC6 were also highly expressed. Fibroblasts were defined by high expression of COL1A1. Using these criteria, cells were grouped into 28 distinct clusters that reflect major cell types and developmental states within the analyzed samples.

As shown previously, [15] five non-neuronal clusters were characterized by genes related to cilia, BMP signaling and proteoglycan. Cilia-bearing cell (CBC) cluster highly expressed cilia-related genes (e.g., NPHP1) and significant enrichment of ‘‘cilium assembly (GO:0060271)’’ (FDR <0.05). BMP-responsible cells (BRC) show substantial expression of

Author Manuscript Author Manuscript Author Manuscript Author Manuscript

BMP pathway genes (MSX1, BMP4) without significant enrichment of ‘‘cilium assembly (GO:0060271)’’. Two non-neuronal clusters expressing extracellular proteoglycans (BGN and DCN). The proteoglycan-expressing clusters without and with ‘‘mitotic nuclear division (GO:0007067)’’ (FDR <0.05) was labeled as proteoglycan-expressing cells (PGC) and progenitor (PGP), respectively. The rest cluster showed no significant enrichment of GO terms and called as an unassigned cluster (UN). The substantial marker expression for cell type assignment satisfies 1.25-fold change and FDR <0.05.

The reference transcriptomes of fetal and adult brain were downloaded from NCBI Short Read Archive (SRP057196). [23] Gene signatures for each cell type was obtained as described previously (Figure S6C). In each cell, genes were ranked by relative expression to average of all cells. Gene Set Enrichment Analysis (GSEA) was conducted by GSEAPY software (v0.9.3) with options ‘‘‘‘–max-size 50000–min-size 0 -n 1000’’ to the pre-sorted genes.

Potential genes involved in neurological diseases were downloaded from DisGeNET database with more than 0.25 confidence score.[24] Enrichment of the disease-related genes was evaluated by GSEA software (v4.0.3).[57] In each experimental condition, genes were pre-ranked by relative average expression of all cells to that from other conditions. GSEA was implemented to the pre-ranked gene list with 100 permutations and without collapse of gene sets.ASD risk genes were downloaded from SFARI. High confident ASD genes (category S, 1 and 2) were used for subsequent differential expression analysis between RF- and non-treated hCOs. Non-SFARI neuronal genes were defined by genes that were related to ‘‘neuron development (GO:0048666)’’, but not listed in SFARI genes. Differential expression levels of ASD risk genes were measured by –log10(*p*-value) with two-sided T test.

Retrotransposon (RT) expression in individual cells was calculated by counting scRNA-seq reads into RT transcripts by count function of CellRanger. Briefly, a reference package for hg19 RT was constructed with hg19 genomic sequence and RT GTF-formatted file by mkref function with default parameters. GTF file showing RT was downloaded from Hammell lab website (http://hammelllab.labsites.cshl.edu/software/). Global RT expression was calculated by dividing UMI count in RT by that in gene in individual cells. Differential expression of RT was analyzed in an RT-enriched neuronal cluster (Neuron4) by two-sided T test between RT- and non-treated hCOs.

Pseudotime trajectory and cell distribution analyses were performed using monocle3 (v1.2.7). The RNA count matrix and metadata were extracted from the integrated Seurat object to create a monocle3 new_cell_data_set, and the UMAP coordinates computed by Seurat were embedded. Next, cluster and trajectory structures were learned using cluster_cells and learn_graph, respectively, and pseudotime was estimated with order_cells. The pseudotime values were obtained via the pseudotime function. Cell distribution comparisons employed ridge plots from the ggridges package, and the expression of genes of interest was visualized against pseudotime using ggplot2 after log(1 + x) transformation.

scATAC-seq data processing and analysis: Single-cell ATAC-seq data were processed using Cell Ranger ATAC outputs (10x Genomics) and analyzed in Seurat (v4.3.0)

Author Manuscript Author Manuscript Author Manuscript Author Manuscript

with the Signac extension. Cells with fewer than 500 passed filters were discarded initially. Custom peak sets were generated by reading individual BED files for each sample, merging overlapping peaks (using the reduce function), and retaining only those within a specified size range (20–10,000 bp). Following the generation of Fragment objects for each sample, fragment counts overlapping the combined peak set were quantified with FeatureMatrix. These counts were used to create ChromatinAssay objects. Quality control included calculating the TSS enrichment score and nucleosome signal, then filtering out cells based on thresholds for total ATAC counts, TSS enrichment, and nucleosome signal.

Next, the three datasets were merged into a single Seurat object. Dimensional reduction was performed using TF-IDF normalization, selection of top features singular value decomposition, and UMAP projection. Cell clustering was conducted with FindNeighbors and FindClusters (resolution = 1). Cell-type labels were assigned via marker gene inspection and coverage visualization, including CoveragePlot over known marker loci.

To integrate of scRNA-seq and scATAC-seq data, Gene activities were computed in the scATAC-seq dataset (using GeneActivity) based on the variable genes identified in the scRNA-seq data. Next, FindTransferAnchors linked scRNA-seq (reference) and scA-TAC-seq (query), allowing cell-type labels to be transferred and stored as metadata in the scATAC-seq object. For co-embedding, both datasets were merged, imputed gene expression in the scATAC-seq cells, and then scaled and visualized via PCA and UMAP. Finally, CoveragePlot was used to compare chromatin accessibility across predicted cell types, providing an integrated view of gene expression and accessibility.

Viral labeling and calcium imaging: As we described previously, [14,15] organoids were transferred to 96-well plate for viral infection. After AAV. syn. GCAMP6s.WPRE. SV40 (Addgene, 100843, [62]) and AAV5.hSyn. eGFP (Addgene, 50465, was a gift from Bryan Roth) separate incubation in 300 μL neural media for 24 h, organoids were transferred to 6-well plate in fresh medium. After 10 to 15 days virus transduction, the intact organoids were used for calcium and structural imaging. Time-lapse images were taken with Leica TCS SP8 confocal microscope at a speed of 1s/frame. Tracings of single cell calcium surges were determined from measuring the region of interest and mean of interest fluorescence intensities using Fiji software.[54] The change in calcium concentration is calculated as follow; $\Delta F/F = [(F(t)-F0)/F0)$, where F0 is calculated as the average of portions without calcium events.

Electrophysiological recordings: Whole-cell patch-clamp recordings were obtained from intact RF-treated hCOs and control hCOs (D100−120; 3 hCOs for each cohort) using artificial cerebrospinal fluid containing (in mM) 126 NaCl, 2.5 KCl, 26 $NaHCO_3$, 2 $CaCl_2$, 2 $MgCl_2$, 1.25 NaH_2PO_4, and 10 glucose gasses with 95% O_2/5% CO_2. Cortical cells were visualized with an upright microscope (Olympus; BX61WI) with infrared differential interference contrast optics and with a water immersion 40x objective. Electrical recordings were obtained from cortical cells with borosilicate glass pipettes (4−6 MΩ) when filled with pipette solution containing (in mM) 126 K-gluconate, 4 KCl, 10 HEPES, 4 ATP-Mg, 0.3 GTP-Na, and 10 phosphocreatine (pH 7.2 and osmolality of 290 mOsm). MultiClamp700B amplifier (Molecular Devices) was used for recordings. Voltage signals were filtered at 3

Author Manuscript Author Manuscript Author Manuscript Author Manuscript

kHz using a Bessel filter and digitized at 10 kHz with Digidata 1440A digitizer (Molecular Devices). Cortical cells were injected with depolarizing current steps (+5 to +40 pA, 5 pA increments, 1 s from −60 mV) in order to evoke action potentials as we previously described (Cakir et al., 2019). The Clampfit 10 software (Molecular Devices) was used to analyze the data. V_{rest}, R_{input}, and $\tau_{membrane}$ were examined as we previously described. [63] (1) Vrest was measured from the average voltage after an equilibration period. (2) Rinput was measured from voltage responses to 1s current steps (−10 to +10 pA, 5 pA increments). The slope of I-V curve was calculated at steady state (0.9–1.0 s from the start of current steps). (3) τmembrane was measured from voltage responses to 1s steps (−5 pA). Single exponential functions were fitted to the voltage responses from the start of current step to the hyperpolarization peak to measure decay time constant.

Real-time quantitative PCR (qPCR): After total RNA was isolated from the whole organoids using RNeasy Mini Kit (Qiagen), 1 μg RNA was converted to cDNA via iScript Select cDNA Synthesis Kit. For the quantification of gene expression, qPCR was carried out on the CFX96 Real-Time PCR system (Biorad) using the SsoFast EvaGreen Supermix (Biorad). The PCR conditions were: 95° C for 15 min, followed by 40 two-step cycles at 94° C for 10 s and 60° C for 45 s. A list of primers used in this study is presented in Table S1.

QUANTIFICATION AND STATISTICAL ANALYSIS

Quantification of immunostaining, qPCR, and neuronal activity was performed using unpaired two-tailed t-tests to determine statistical significance. For multiple comparisons, multiple t-tests were applied as appropriate. Mean values ±standard deviation (SD) is reported unless otherwise stated. The sample size (n) represents at least three independent biological replicates. All statistical analyses were conducted using GraphPad Prism 10. For all statistical analyses, *p* value less than 0.05 was interpreted as statistically significant. The statistical details of experiments can also be found in the figure legends and corresponding results.

Supplementary Material

Refer to Web version on PubMed Central for supplementary material.

ACKNOWLEDGMENTS

We thank Cheryl Sousa Kim for helpful discussion and all staff members of the Yale Center for Genome Analysis. I.-H.P. was partly supported by NIH (R01MH118344–01A1), the Simons Foundation, and the NOMIS Foundation. Computation time was provided by the Yale University Biomedical High Performance Computing Center. P.R. was supported by NIDA grant R37DA023999–12.

REFERENCES

1. Andrews MG, Subramanian L, Salma J, and Kriegstein AR (2022). How mechanisms of stem cell polarity shape the human cerebral cortex. Nat. Rev. Neurosci. 23, 711–724. 10.1038/s41583-022-00631-3. [PubMed: 36180551]
2. Willsey HR, Willsey AJ, Wang B, and State MW (2022). Genomics, convergent neuroscience and progress in understanding autism spectrum disorder. Nat. Rev. Neurosci. 23, 323–341. 10.1038/s41583-022-00576-7. [PubMed: 35440779]

Author Manuscript Author Manuscript Author Manuscript Author Manuscript

3. Elsabbagh M, Divan G, Koh YJ, Kim YS, Kauchali S, Marcn C, Montiel-Nava C, Patel V, Paula CS, Wang C, et al. (2012). Global prevalence of autism and other pervasive developmental disorders. Autism Res. 5, 160–179. 10.1002/aur.239. [PubMed: 22495912]

4. Gilissen C, Hehir-Kwa JY, Thung DT, van de Vorst M, van Bon BWM, Willemsen MH, Kwint M, Janssen IM, Hoischen A, Schenck A, et al. (2014). Genome sequencing identifies major causes of severe intellectual disability. Nature 511, 344–347. 10.1038/nature13394. [PubMed: 24896178]

5. Silbereis JC, Pochareddy S, Zhu Y, Li M, and Sestan N (2016). The Cellular and Molecular Landscapes of the Developing Human Central Nervous System. Neuron 89, 248–268. 10.1016/j.neuron.2015.12.008. [PubMed: 26796689]

6. Love C, Sominsky L, O'Hely M, Berk M, Vuillermin P, and Dawson SL (2024). Prenatal environmental risk factors for autism spectrum disorder and their potential mechanisms. BMC Med. 22, 393. 10.1186/s12916-024-03617-3. [PubMed: 39278907]

7. Tooley UA, Bassett DS, and Mackey AP (2021). Environmental influences on the pace of brain development. Nat. Rev. Neurosci. 22, 372–384. 10.1038/s41583-021-00457-5. [PubMed: 33911229]

8. Huss A, Dongus S, Aminzadeh R, Thielens A, van den Bossche M, Van Torre P, de Seze R, Cardis E, Eeftens M, Joseph W, et al. (2021). Exposure to radiofrequency electromagnetic fields: Comparison of exposimeters with a novel body-worn distributed meter. Environ. Int. 156, 106711. 10.1016/j.envint.2021.106711.

9. Manna D, and Ghosh R (2016). Effect of radiofrequency radiation in cultured mammalian cells: A review. Electromagn. Biol. Med. 35, 265–301. 10.3109/15368378.2015.1092158. [PubMed: 27053138]

10. Eghlidospour M, Ghanbari A, Mortazavi SMJ, and Azari H (2017). Effects of radiofrequency exposure emitted from a GSM mobile phone on proliferation, differentiation, and apoptosis of neural stem cells. Anat. Cell Biol. 50, 115–123. 10.5115/acb.2017.50.2.115.

11. Chiaradia I, and Lancaster MA (2020). Brain organoids for the study of human neurobiology at the interface of in vitro and in vivo. Nat. Neurosci. 23, 1496–1508. 10.1038/s41593-020-00730-3. [PubMed: 33139941]

12. Lancaster MA, and Knoblich JA (2014). Organogenesis in a dish: modeling development and disease using organoid technologies. Science 345, 1247125. 10.1126/science.1247125.

13. Pasca SP (2018). The rise of three-dimensional human brain cultures. Nature 553, 437–445. 10.1038/nature25032. [PubMed: 29364288]

14. Cakir B, Xiang Y, Tanaka Y, Kural MH, Parent M, Kang YJ, Chapeton K, Patterson B, Yuan Y, He CS, et al. (2019). Engineering of human brain organoids with a functional vascular-like system. Nat. Methods 16, 1169–1175. 10.1038/s41592-019-0586-5. [PubMed: 31591580]

15. Xiang Y, Tanaka Y, Patterson B, Kang YJ, Govindaiah G, Roselaar N, Cakir B, Kim KY, Lombroso AP, Hwang SM, et al. (2017). Fusion of Regionally Specified hPSC-Derived Organoids Models Human Brain Development and Interneuron Migration. Cell Stem Cell 21, 383–398.e7. 10.1016/j.stem.2017.07.007. [PubMed: 28757360]

16. Micali N, Kim SK, Diaz-Bustamante M, Stein-O'Brien G, Seo S, Shin JH, Rash BG, Ma S, Wang Y, Olivares NA, et al. (2020). Variation of Human Neural Stem Cells Generating Organizer States In Vitro before Committing to Cortical Excitatory or Inhibitory Neuronal Fates. Cell Rep. 31, 107599. 10.1016/j.celrep.2020.107599.

17. Lancaster MA, Corsini NS, Wolfinger S, Gustafson EH, Phillips AW, Burkard TR, Otani T, Livesey FJ, and Knoblich JA (2017). Guided self-organization and cortical plate formation in human brain organoids. Nat. Biotechnol. 35, 659–666. 10.1038/nbt.3906. [PubMed: 28562594]

18. Watanabe K, Kamiya D, Nishiyama A, Katayama T, Nozaki S, Kawasaki H, Watanabe Y, Mizuseki K, and Sasai Y (2005). Directed differentiation of telencephalic precursors from embryonic stem cells. Nat. Neurosci. 8, 288–296. 10.1038/nn1402. [PubMed: 15696161]

19. Rakic P (1988). Specification of cerebral cortical areas. Science 241, 170–176. 10.1126/science.3291116. [PubMed: 3291116]

20. Rakic P (2009). Evolution of the neocortex: a perspective from developmental biology. Nat. Rev. Neurosci. 10, 724–735. 10.1038/nrn2719. [PubMed: 19763105]

21. Bershteyn M, Nowakowski TJ, Pollen AA, Di Lullo E, Nene A, Wynshaw-Boris A, and Kriegstein AR (2017). Human iPSC-Derived Cerebral Organoids Model Cellular Features of Lissencephaly

Author Manuscript Author Manuscript Author Manuscript Author Manuscript

and Reveal Prolonged Mitosis of Outer Radial Glia. Cell Stem Cell 20, 435–449.e4. 10.1016/j.stem.2016.12.007. [PubMed: 28111201]

22. Schulz RB, Plantz VC, and Brush DR (1988). Shielding Theory and Practice. IEEE T Electromagn. C 30, 187–201. 10.1109/15.3297.
23. Darmanis S, Sloan SA, Zhang Y, Enge M, Caneda C, Shuer LM, Hayden Gephart MG, Barres BA, and Quake SR (2015). A survey of human brain transcriptome diversity at the single cell level. Proc. Natl. Acad. Sci. USA 112, 7285–7290. 10.1073/pnas.1507125112. [PubMed: 26060301]
24. Pinero J, Bravo À, Queralt-Rosinach N, Gutiérrez-Sacristán A, DeuPons J, Centeno E, García-García J, Sanz F, and Furlong LI (2017). DisGeNET: a comprehensive platform integrating information on human disease-associated genes and variants. Nucleic Acids Res. 45, D833–D839. 10.1093/nar/gkw943. [PubMed: 27924018]
25. Abrahams BS, Arking DE, Campbell DB, Mefford HC, Morrow EM, Weiss LA, Menashe I, Wadkins T, Banerjee-Basu S, and Packer A (2013). SFARI Gene 2.0: a community-driven knowledgebase for the autism spectrum disorders (ASDs). Mol. Autism 4, 36. 10.1186/2040-2392-4-36. [PubMed: 24090431]
26. Parras A, Anta H, Santos-Galindo M, Swarup V, Elorza A, Nieto-González JL, Picó S, Hernández IH, Díaz-Hernández JI, Belloc E, et al. (2018). Autism-like phenotype and risk gene mRNA deadenylation by CPEB4 mis-splicing. Nature 560, 441–446. 10.1038/s41586-018-0423-5. [PubMed: 30111840]
27. Shpyleva S, Melnyk S, Pavliv O, Pogribny I, and Jill James S (2018). Overexpression of LINE-1 Retrotransposons in Autism Brain. Mol. Neurobiol. 55, 1740–1749. 10.1007/s12035-017-0421-x. [PubMed: 28220356]
28. Jacob-Hirsch J, Eyal E, Knisbacher BA, Roth J, Cesarkas K, Dor C, Farage-Barhom S, Kunik V, Simon AJ, Gal M, et al. (2018). Whole-genome sequencing reveals principles of brain retrotransposition in neurodevelopmental disorders. Cell Res. 28, 187–203. 10.1038/cr.2018.8. [PubMed: 29327725]
29. Xiang Y, Fanaka Y, Patterson B, Hwang SM, Hysolli E, Cakir B, Kim KY, Wang W, Kang YJ, Clement EM, Zhong M, et al. (2020). Dysregulation of BRD4 Function Underlies the Functional Abnormalities of MeCP2 Mutant Neurons. Mol. Cell 79, 84. 10.1016/j.molcel.2020.05.016. [PubMed: 32526163]
30. Susaimanickam PJ, Kiral FR, and Park IH (2022). Region Specific Brain Organoids to Study Neurodevelopmental Disorders. Int. J. Stem Cells 15, 26–40. 10.15283/ijsc22006. [PubMed: 35220290]
31. Dixon TA, and Muotri AR (2023). Advancing preclinical models of psychiatric disorders with human brain organoid cultures. Mol. Psychiatry 28, 83–95. 10.1038/s41380-022-01708-2. [PubMed: 35948659]
32. Wu Y, De Asis-Cruz J, and Limperopoulos C (2024). Brain structural and functional outcomes in the offspring of women experiencing psychological distress during pregnancy. Mol. Psychiatry 29, 2223–2240. 10.1038/s41380-024-02449-0. [PubMed: 38418579]
33. Depla JA, Mulder LA, de Sá RV, Wartel M, Sridhar A, Evers MM, Wolthers KC, and Pajkrt D (2022). Human Brain Organoids as Models for Central Nervous System Viral Infection. Viruses 14, 634. 10.3390/v14030634. [PubMed: 35337041]
34. Li K, Gu L, Cai H, Lu HC, Mackie K, and Guo F (2025). Human brain organoids for understanding substance use disorders. Drug Metab. Pharmacokinet. 60, 101036. 10.1016/j.dmpk.2024.101036.
35. Notaras M, Lodhi A, Barrio-Alonso E, Foord C, Rodrick T, Jones D, Fang H, Greening D, and Colak D (2021). Neurodevelopmental signatures of narcotic and neuropsychiatric risk factors in 3D human-derived forebrain organoids. Mol. Psychiatry 26, 7760–7783. 10.1038/s41380-021-01189-9. [PubMed: 34158620]
36. Arzua T, Yan Y, Jiang C, Logan S, Allison RL, Wells C, Kumar SN, Schäfer R, and Bai X (2020). Modeling alcohol-induced neurotoxicity using human induced pluripotent stem cell-derived three-dimensional cerebral organoids. Transl. Psychiatry 10, 347. 10.1038/s41398-020-01029-4. [PubMed: 33051447]

Author Manuscript Author Manuscript Author Manuscript Author Manuscript

37. Noctor SC, Martínez-Cerdeño V, Ivic L, and Kriegstein AR (2004). Cortical neurons arise in symmetric and asymmetric division zones and migrate through specific phases. Nat. Neurosci. 7, 136–144. 10.1038/nn1172. [PubMed: 14703572]
38. Benito-Kwiecinski S, Giandomenico SL, Sutcliffe M, Riis ES, Freire-Pritchett P, Kelava I, Wunderlich S, Martin U, Wray GA, McDole K, and Lancaster MA (2021). An early cell shape transition drives evolutionary expansion of the human forebrain. Cell 184, 2084–2102.e19. 10.1016/j.cell.2021.02.050. [PubMed: 33765444]
39. Subramanian L, Bershteyn M, Paredes MF, and Kriegstein AR (2017). Dynamic behaviour of human neuroepithelial cells in the developing forebrain. Nat. Commun. 8, 14167. 10.1038/ncomms14167. [PubMed: 28139695]
40. Ni Y, Mulier S, Miao Y, Michel L, and Marchal G (2005). A review of the general aspects of radiofrequency ablation. Abdom. Imaging 30, 381–400. 10.1007/s00261-004-0253-9. [PubMed: 15776302]
41. Aldad TS, Gan G, Gao XB, and Taylor HS (2012). Fetal radiofrequency radiation exposure from 800–1900 mhz-rated cellular telephones affects neurodevelopment and behavior in mice. Sci. Rep. 2, 312. 10.1038/srep00312. [PubMed: 22428084]
42. Di Lullo E, and Kriegstein AR (2017). The use of brain organoids to investigate neural development and disease. Nat. Rev. Neurosci. 18, 573–584. 10.1038/nrn.2017.107. [PubMed: 28878372]
43. Heyer DB, and Meredith RM (2017). Environmental toxicology: Sensitive periods of development and neurodevelopmental disorders. Neurotoxicology 58, 23–41. 10.1016/j.neuro.2016.10.017. [PubMed: 27825840]
44. Ang ESBC Jr., Gluncic V, Duque A, Schafer ME, and Rakic P (2006). Prenatal exposure to ultrasound waves impacts neuronal migration in mice. Proc. Natl. Acad. Sci. USA 103, 12903–12910. 10.1073/pnas.0605294103. [PubMed: 16901978]
45. Nishiyama J (2019). Plasticity of dendritic spines: Molecular function and dysfunction in neurodevelopmental disorders. Psychiatry Clin. Neurosci. 73, 541–550. 10.1111/pcn.12899. [PubMed: 31215705]
46. Servadio M, Vanderschuren LJMJ, and Trezza V (2015). Modeling autism-relevant behavioral phenotypes in rats and mice: Do 'autistic' rodents exist? Behav. Pharmacol. 26, 522–540. 10.1097/FBP.0000000000000163. [PubMed: 26226143]
47. Kreiborg S, and Cohen MM Jr. (1991). The infant Apert skull. Neuro-surg. Clin. N. Am. 2, 551–554.
48. Zhou Y, Song H, and Ming GL (2024). Genetics of human brain development. Nat. Rev. Genet. 25, 26–45. 10.1038/s41576-023-00626-5. [PubMed: 37507490]
49. Andrews MG, and Kriegstein AR (2022). Challenges of Organoid Research. Annu. Rev. Neurosci. 45, 23–39. 10.1146/annurev-neuro-111020-090812. [PubMed: 34985918]
50. Cakir B, Kiral FR, and Park IH (2022). Advanced in vitro models: Microglia in action. Neuron 110, 3444–3457. 10.1016/j.neuron.2022.10.004. [PubMed: 36327894]
51. Cakir B, Tanaka Y, Kiral FR, Xiang Y, Dagliyan O, Wang J, Lee M, Greaney AM, Yang WS, duBoulay C, et al. (2022). Expression of the transcription factor PU.1 induces the generation of microglia-like cells in human cortical organoids. Nat. Commun. 13, 430. 10.1038/s41467-022-28043-y. [PubMed: 35058453]
52. Xiang Y, Tanaka Y, Cakir B, Patterson B, Kim K-Y, Sun P, Kang Y-J, Zhong M, Liu X, Patra P, et al. (2019). hESC-Derived Thalamic Organoids Form Reciprocal Projections When Fused with Cortical Organoids. Cell Stem Cell 24, 487–497.e7. 10.1016/j.stem.2018.12.015. [PubMed: 30799279]
53. Verbeek J, Oftedal G, Feychting M, van Rongen E, Rosaria Scarfì M, Mann S, Wong R, and van Deventer E (2021). Prioritizing health outcomes when assessing the effects of exposure to radiofrequency electromagnetic fields: A survey among experts. Environ. Int. 146, 106300. 10.1016/j.envint.2020.106300.
54. Schindelin J, Arganda-Carreras I, Frise E, Kaynig V, Longair M, Pietzsch T, Preibisch S, Rueden C, Saalfeld S, Schmid B, et al. (2012). Fiji: an open-source platform for biological-image analysis. Nat. Methods 9, 676–682. 10.1038/nmeth.2019. [PubMed: 22743772]

Author Manuscript Author Manuscript Author Manuscript Author Manuscript

55. Stuart T, Butler A, Hoffman P, Hafemeister C, Papalexi E, Mauck WM 3rd, Hao Y, Stoeckius M, Smibert P, and Satija R (2019). Comprehensive Integration of Single-Cell Data. Cell 177, 1888–1902.e21. 10.1016/j.cell.2019.05.031. [PubMed: 31178118]

56. Falcon S, and Gentleman R (2007). Using GOstats to test gene lists for GO term association. Bioinformatics 23, 257–258. 10.1093/bioinformatics/btl567. [PubMed: 17098774]

57. Subramanian A, Tamayo P, Mootha VK, Mukherjee S, Ebert BL, Gillette MA, Paulovich A, Pomeroy SL, Golub TR, Lander ES, and Mesirov JP (2005). Gene set enrichment analysis: a knowledge-based approach for interpreting genome-wide expression profiles. Proc. Natl. Acad. Sci. USA 102, 15545–15550. 10.1073/pnas.0506580102. [PubMed: 16199517]

58. Trapnell C, Pachter L, and Salzberg SL (2009). TopHat: discovering splice junctions with RNA-Seq. Bioinformatics 25, 1105–1111. 10.1093/bioinformatics/btp120. [PubMed: 19289445]

59. Trapnell C, Williams BA, Pertea G, Mortazavi A, Kwan G, van Baren MJ, Salzberg SL, Wold BJ, and Pachter L (2010). Transcript assembly and quantification by RNA-Seq reveals unannotated transcripts and isoform switching during cell differentiation. Nat. Biotechnol. 28, 511–515. 10.1038/nbt.1621. [PubMed: 20436464]

60. Androutsellis-Theotokis A, Murase S, Boyd JD, Park DM, Hoeppner DJ, Ravin R, and McKay RDG (2008). Generating neurons from stem cells. Methods Mol. Biol. 438, 31–38. 10.1007/978-1-59745-133-8_4. [PubMed: 18369747]

61. Ravin R, Hoeppner DJ, Munno DM, Carmel L, Sullivan J, Levitt DL, Miller JL, Athaide C, Panchision DM, and McKay RDG (2008). Potency and fate specification in CNS stem cell populations in vitro. Cell Stem Cell 3, 670–680. 10.1016/j.stem.2008.09.012. [PubMed: 19041783]

62. Chen T-W, Wardill TJ, Sun Y, Pulver SR, Renninger SL, Baohan A, Schreiter ER, Kerr RA, Orger MB, Jayaraman V, et al. (2013). Ultrasensitive fluorescent proteins for imaging neuronal activity. Nature 499, 295–300. 10.1038/nature12354. [PubMed: 23868258]

63. Kang YJ, Clement EM, Park IH, Greenfield LJ Jr., Smith BN, and Lee SH (2021). Vulnerability of cholecystokinin-expressing GABAergic interneurons in the unilateral intrahippocampal kainate mouse model of temporal lobe epilepsy. Exp. Neurol. 342, 113724. 10.1016/j.expneurol.2021.113724. [PubMed: 33915166]

Author Manuscript Author Manuscript Author Manuscript Author Manuscript

Highlights

- RF exposure alters radial glial differentiation in human cortical organoids
- RF induces ASD-related gene and retroelement expression in cortical organoids
- BET protein dysregulation mediates RF-induced neurodevelopmental defects
- BET inhibitors rescue RF-induced developmental defects in cortical organoids

Author Manuscript Author Manuscript Author Manuscript Author Manuscript

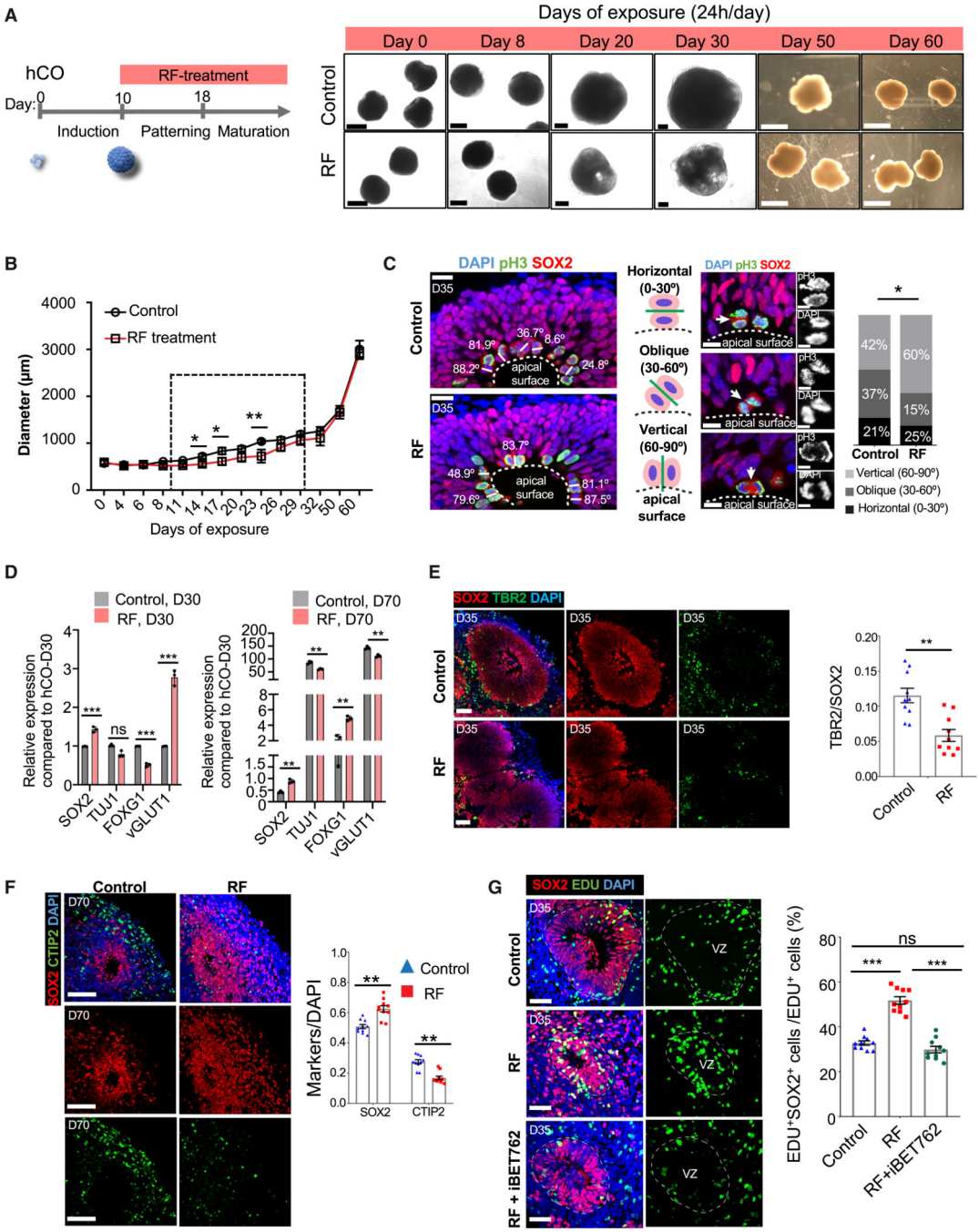


Figure 1. RF treatment distorts human cortical organization

(A) Left, schematic for generating hCOs from hESCs with radiation as described in Xiang et al. [15] Starting from the beginning of the patterning stage, hCOs are exposed to 24 h/day RF throughout their development. Right, representative bright-field images of age-matched organoids with and without RF treatment.

(B) Quantification of the average organoid diameter over the course of hCO development. Data represent the mean ± SEM (n = 100 organoids, the unpaired two-tailed t test was used

Author Manuscript Author Manuscript Author Manuscript Author Manuscript

for all comparisons; 14-day exposure: T = 27.38, df = 198, *$p < 0.05$ and **$p < 0.01$ from three hESC lines and five independent batches).

(C) Left, co-immunostaining for phospho-histone H3 and SOX2 in hCO sections (5 weeks old). Middle, representative images of vertical, oblique, and horizontal cleavage of dividing RGs in ventricular zone-like area. Right, quantification of mitotic behaviors of SOX2+ RGs with and without RF treatment. Data represent the mean ± SEM ($p < 0.05$, $n = 55$ organoids, from three hESC lines and three independent batches; an unpaired two-tailed t test with Welch's correction was used for comparison).

(D) Expression of cortical genes from hCOs with and without RF treatment (30 and 70 days old). Gene expression was measured relative to control organoids on day 30 and normalized to β-actin. Data represent the mean ± SEM ($n = 15$ organoids, a multiple t test was used for all comparisons, T = 7.141, df = 4.00, **$p < 0.01$ and ***$p < 0.001$, from three independent batches.).

(E and F) Immunostaining of hCOs with and without RF treatment for SOX2 and TBR2 (E) SOX2 and CTIP2 (F). Right, quantification of cortical plate-like area markers. Data represent the mean ± SEM ($p < 0.01$, $n = 10$ organoids, a multiple t test was used for all comparisons, T = 8.430, df = 4.00, **$p < 0.01$, from three independent batches).

(G) Left: confocal images for EdU pulse-chase experiments, with newborn RG cells labeled with SOX2 and EdU within progenitor zone (VZ) without and with iBET762 treatment. The scale bar represents 50 μm. Right: quantification of Edu+SOX2+ cells over EdU+ cells. Data represent the mean ± SEM (***$p < 0.0001$, $n = 10$ organoids, from three independent batches). An unpaired two-tailed t test with Welch's correction was used for all comparisons. The scale bar represents 20, 10, and 5 μm in (C), left to right, and 50 μm in (E) and (F).

Author Manuscript Author Manuscript Author Manuscript Author Manuscript

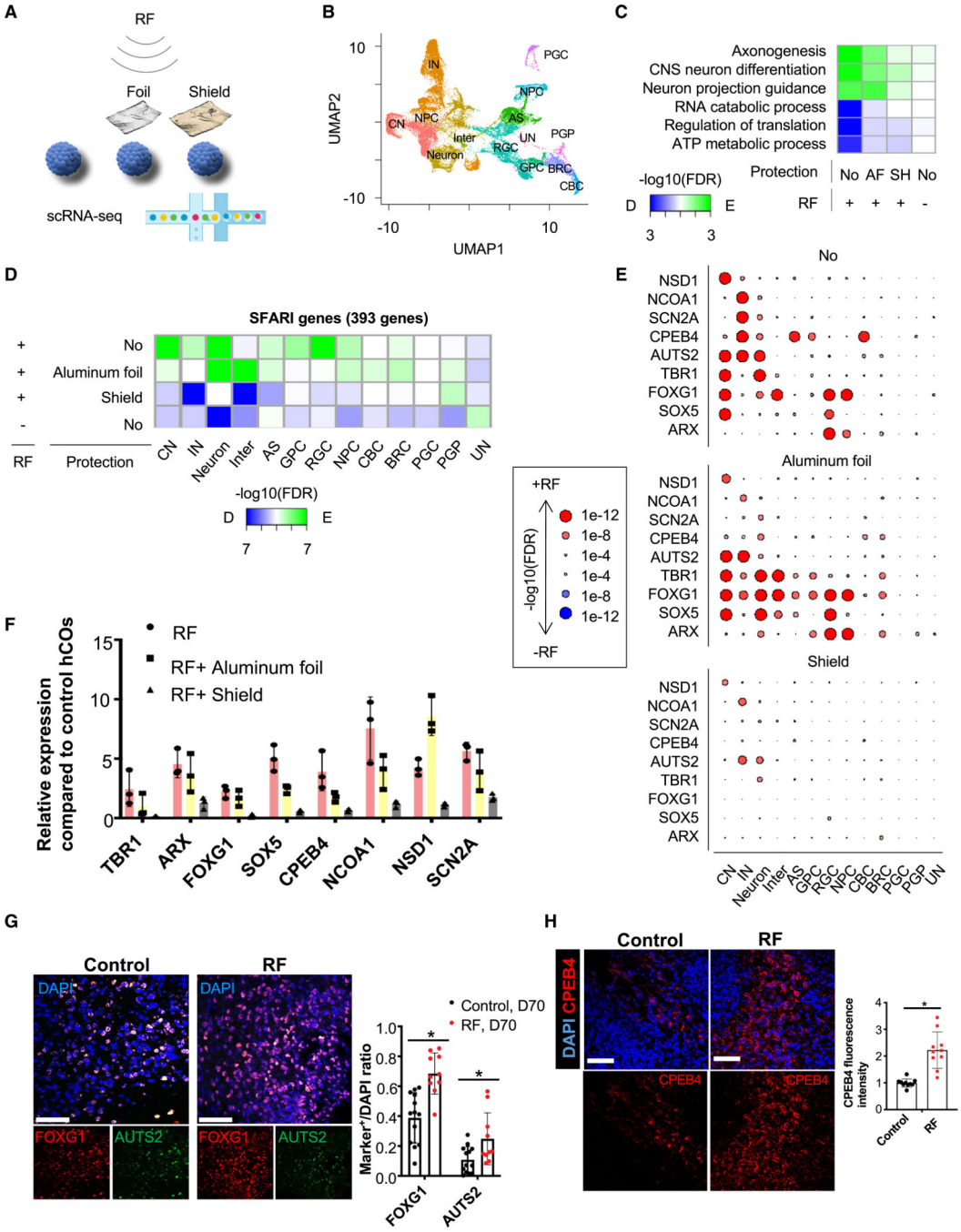


Figure 2. Single-cell transcriptome analysis of RF-treated hCOs

(A) Strategy of scRNA-seq for hCOs with RF exposure with or without shield (SH) or aluminum foil (AF).

(B) UMAP plot of single cells from RF-treated and non-treated hCOs with SH, colored by cell type.

(C) Gene Ontology analysis for global differentially expressed genes in RF-treated hCOs compared to non-treated hCOs. Up- and downregulated GO terms are colored with green and blue, respectively.

Author Manuscript Author Manuscript Author Manuscript Author Manuscript

(D) GSEA of SFARI genes across experimental conditions in each cell type. Enrichment and depletion are colored with green and blue, respectively.
(E) Differential expression of representative SFARI genes between RF-treated and non-treated hCOs. Statistical significance (−log10(FDR)) is shown by circle size. Up- and downregulation in RF-treated hCOs are colored with red and blue, respectively.
(F) Expression of ASD genes from hCOs with RF treatment covered by AF or electromagnetic SH. Gene expression was measured relative to control organoids and normalized to β-actin. Data represent the mean ± SEM ($n = 3$, from three independent batches).
(G) Left, co-immunostaining of hCOs with and without RF treatment for FOXG1 and AUTS2. Right, quantification of markers relative to DAPI.
(H) Left, immunostaining of hCOs with and without RF treatment for CPEB4. Right, quantification of total CPEB4 signal intensity. Data represent the mean ± SEM (*$p < 0.05$, $n = 10$ organoids, from three independent batches). An unpaired two-tailed t test with Welch's correction was used for all comparisons.
The scale bar represents 50 μm in (G) and (H).

Author Manuscript Author Manuscript Author Manuscript Author Manuscript

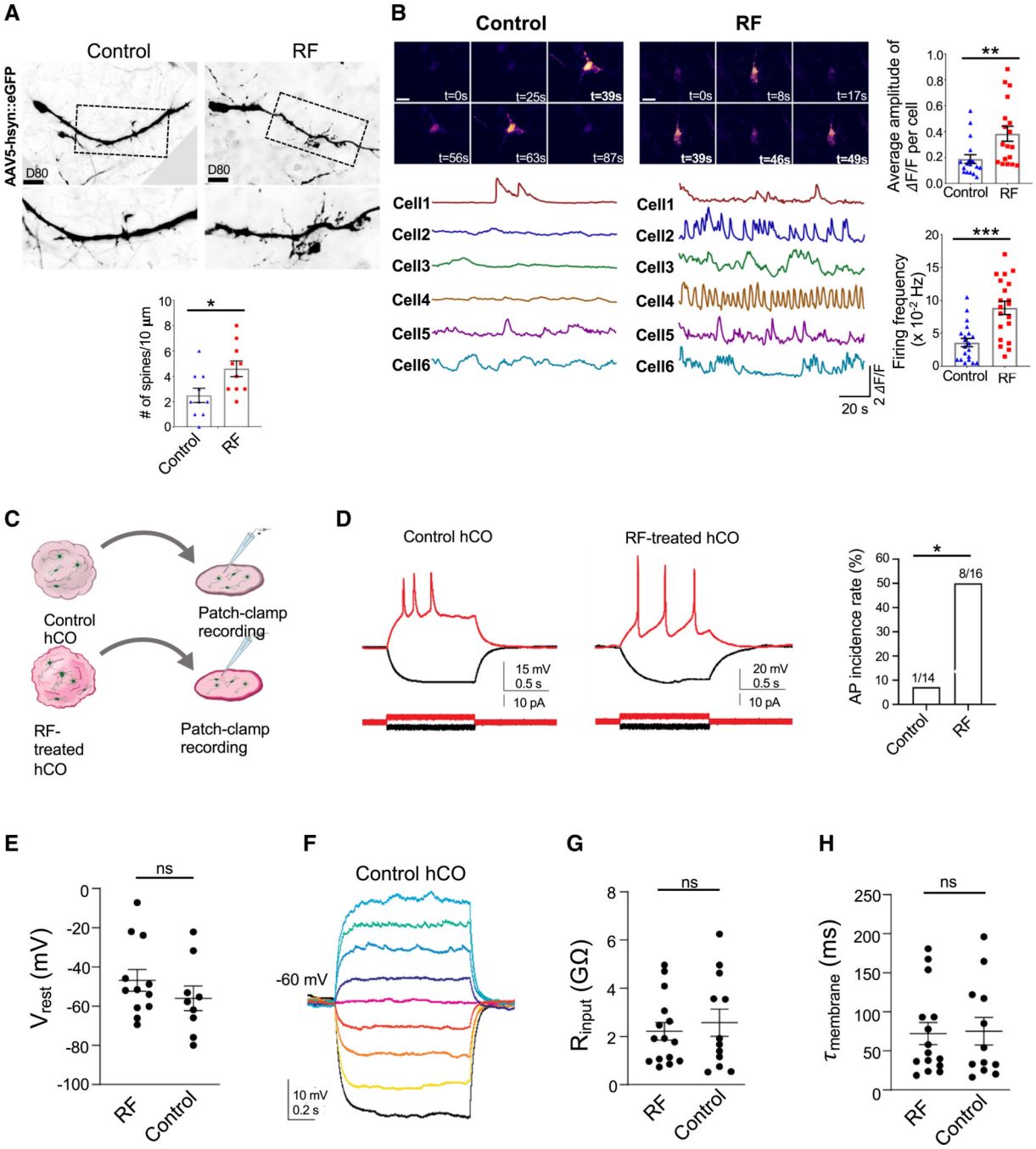


Figure 3. Altered functional properties of neurons under RF treatment

(A) Top, dendritic spine morphology in control and RF-treated hCOs labeled with AAV5-hsyn::EGFP. Bottom, quantification of the number of dendritic spines per 10 µm. Data represent the mean ± SEM (days 75–80, *$p < 0.05$, $n = 10$ organoids, from three independent batches).

(B) Top, representative images demonstrating calcium transient traces observed from individual neurons of control and RF-treated hCOs (days 78–85). Bottom, the single-cell tracings of calcium transient recorded in control and RF-treated organoids. Right, average

Author Manuscript Author Manuscript Author Manuscript Author Manuscript

amplitude of ΔF/F per cell and firing frequency of neurons from control and RF-treated hCOs. Data represent the mean ± SEM (**$p < 0.01$ and ***$p < 0.001$ $n = 20$ organoids, from three independent batches).

(C) Schematic diagram showing whole-cell patch-clamp recording in organoids.

(D) Left, evoked action potentials and voltage responses in cortical cells from RF-treated hCOs and control hCOs by 1-s depolarizing current step (+5 pA) and hyperpolarizing current step (−5 pA). Both cells were held at −60 mV before current steps. Right, bar graph shows the difference in action potential incidence rates between RF-treated hCOs and control hCOs (*$p < 0.05$).

(E) Summary of V_{rest}.

(F) Voltage responses in a neuron from hCO by 1-s current steps (from −20 to +20 pA, +5 pA increments).

(G and H) Summary of R_{nput} (G) and $\tau_{membrane}$ (H). Solid circles and lines indicate individual neurons and averages, respectively. Error bars represent SEM; ns, not significant. An unpaired two-tailed t test with Welch's correction was used for all comparisons.

Author Manuscript Author Manuscript Author Manuscript Author Manuscript

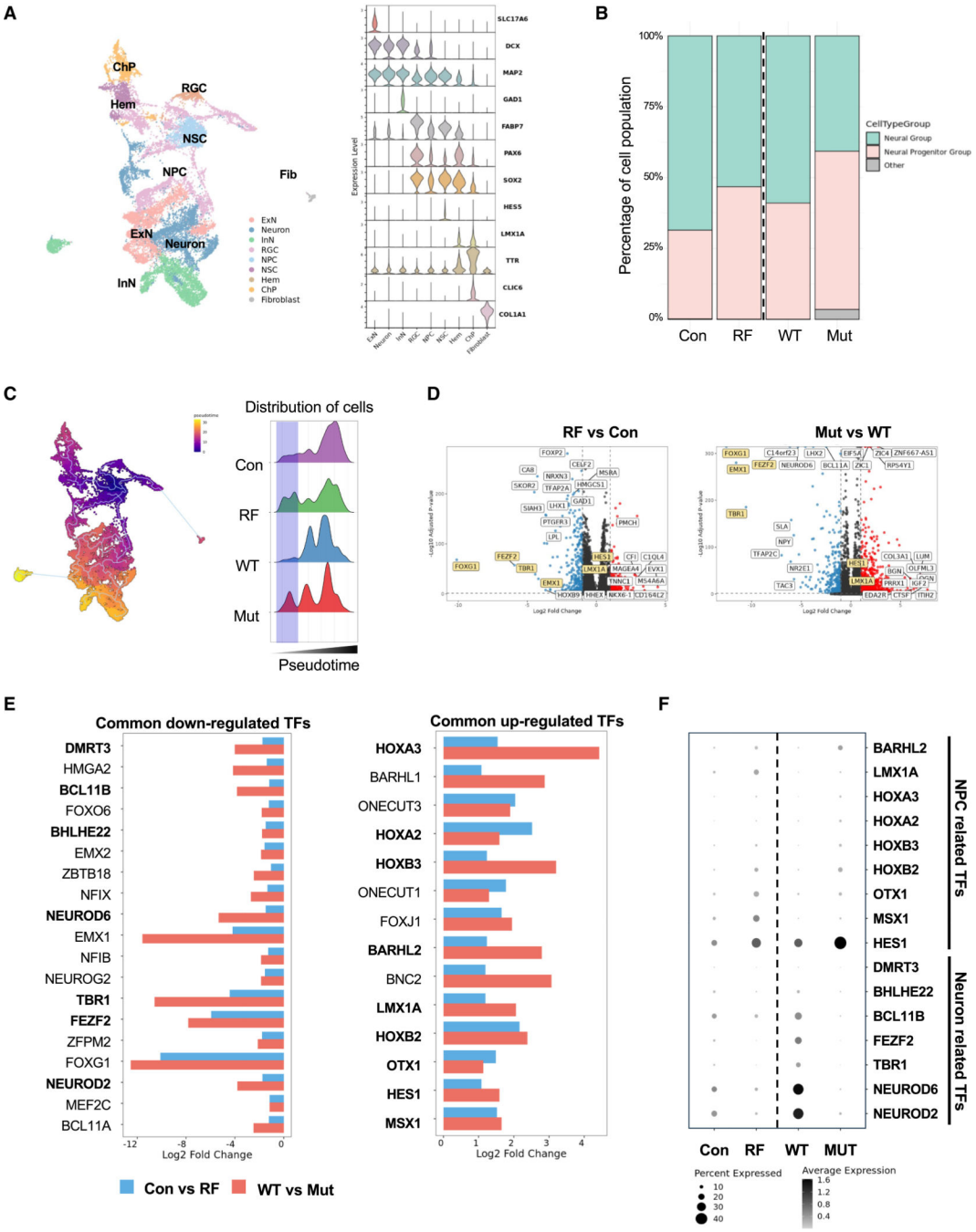


Figure 4. Altered NPC population phenotypes in RF hCOs are similar to those of R113C hCOs

(A) Integrated UMAP plot of single cells from non-treated, RF-treated, wild-type, and R113C COs colored by cell type.

(B) Bar plots for percentage of cell populations in non-treated, RF-treated, wild-type, and R113C COs.

(C) Left, monocle pseudotime trajectory with integrated UMAP embedding of non-treated, RF-treated, wild-type, and R113C COs. Right, prominent cell distributions according to pseudotime changes in non-treated, RF-treated, wild-type, and R113C COs.

Author Manuscript Author Manuscript Author Manuscript Author Manuscript

(D) Volcano plots of differential gene expressions in RF-treated versus non-treated and R113C versus wild-type COs. Genes colored red are significantly increased in the RF-treated or R11C group, and genes colored blue are decreased in the RF-treated or R11C group.

(E) Bar plot for commonly regulated transcription factors (TFs) in non-treated, RF-treated, wild-type, and R113C COs. Bold characters indicate neuron-related TFs (left) and NPC-related TFs (right).

(F) Dot plot of commonly regulated TFs in non-treated, RF-treated, wild-type, and R113C COs. Darker shades of black and the size of dots represent greater expression of genes and the percentage of cells expressing the gene, respectively.

Author Manuscript Author Manuscript Author Manuscript Author Manuscript

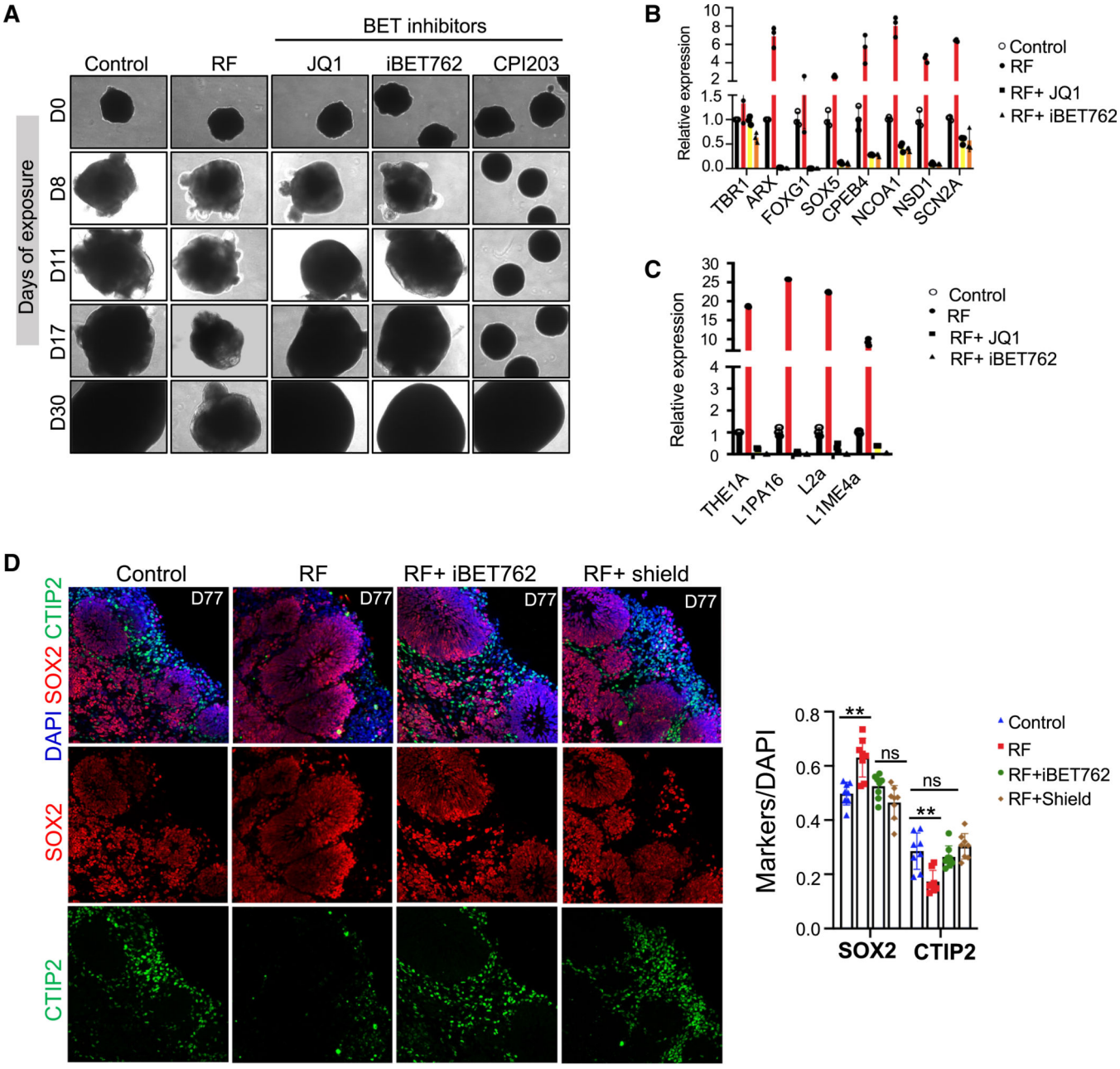


Figure 5. Rescue of RF-induced damage by BET inhibitors

(A) Representative bright-field images of age-matched organoids under RF exposure in the presence and absence of BET inhibitors.

(B and C) Expression of ASD genes (B) and retrotransposon (RT; C) from hCOs under RF exposure in the presence and absence of JQ1 or iBET762. Gene expression was measured relative to control organoids and normalized to β-actin. Data represent the mean ± SEM (n = 15 organoids, from three independent batches).

(D) Left, immunostaining of hCOs under RF exposure in the presence of iBET762 or shield protection for SOX2 and CTIP2. Right, quantification of cortical plate-like area markers. Data represent the mean ± SEM (**$p < 0.01$, n = 8 organoids, from three independent

batches). An unpaired two-tailed t test with Welch's correction was used for all comparisons. The scale bar represents 50 μm.

Author Manuscript Author Manuscript Author Manuscript Author Manuscript

Author Manuscript Author Manuscript Author Manuscript Author Manuscript

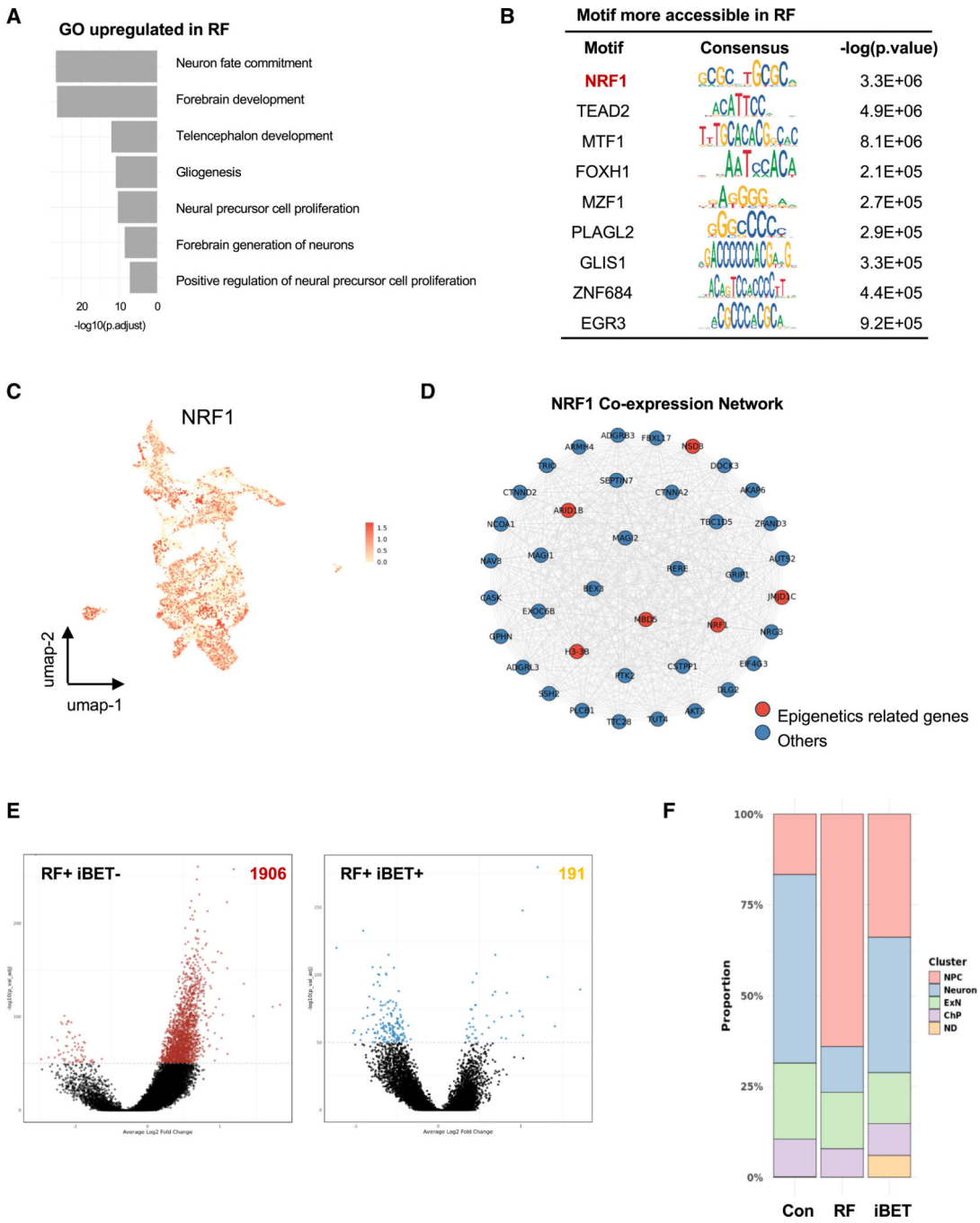


Figure 6. Epigenetic alterations by RF treatment and rescue with iBET in hCOs

(A) Selective GO biological process (BP) enrichment analysis of open-chromatin gene list from RF-treated hCOs.

(B) Motif enrichment analysis of promoter regions in open-chromatin gene list of RF-treated samples.

(C) Feature plot showing the expression of NRF1 genes. Darker red represents the greater expression of each gene.

(D) NRF1 co-expression network analysis in scRNA-seq dataset.

(E) Volcano plots of differential chromatin accessibility in RF- or RF/iBET-treated versus non-treated hCOs. Genes colored red or blue are significantly altered.
(F) Recovery of neuron clusters in RF-treated hCOs by iBET treatment.

Author Manuscript Author Manuscript Author Manuscript Author Manuscript

Author Manuscript Author Manuscript Author Manuscript Author Manuscript

Cell Rep. Author manuscript; available in PMC 2026 March 04.

KEY RESOURCES TABLE

REAGENT or RESOURCE	SOURCE	IDENTIFIER
Antibodies		
MAP2	Millipore	Cat# MAB3418;RRID:AB_94856
phospho-Histone H3	Millipore	Cat# 06–570;RRID:AB_310177
TBR2	R&D Systems	Cat# MAB6166;RRID:AB_10919889
FOXG1	Abcam	Cat# ab196868;RRID:AB_2892604
AUTS2	ThermoFisher	Cat# MA5–31446;RRID:AB_2787082
CPEB4	ThermoFisher	Cat# PA5–58371;RRID:AB_2640115
SATB2	Abcam	Cat# ab92446;RRID:AB_10563678
CTIP2 (25B6)	Abcam	Cat# ab18465;RRID:AB_2064130
SOX2	R&D Systems	Cat# AF2018;RRID:AB_355110
Chemicals, peptides, and recombinant proteins		
mTeSR1	Stem Cell Technologies	Cat# 05875
DMEM-F12	Life Technologies	Cat# 11330057
Neurobasal Media	Life Technologies	Cat# 2110349
FBS	Life Technologies	Cat# 10437028
Amino acids, non-essential	Life Technologies	Cat# 11140050
Penicillin/Streptomycin	Life Technologies	Cat# 15140–122
Glutamax	Life Technologies	Ca# 35050
β-Mercaptoethanol	Sigma	Ca# M7522
N2	Life Technologies	Cat# 17502–048
B27	Life Technologies	Cat# 17504–044
B27 supplement without vitamin A	Life Technologies	Cat# 12587010
bFGF	Millipore	Cat# GF003AF
KnockOut Serum Replacement	Life Technologies	Cat# 10828–028
HBSS	Life Technologies	Cat# 14170112
Matrigel	BD	Cat# 354230
Poly-D-Lysine	Xona	Cat# XC PDL
Y-27632	Stem Cell Technologies	Cat# 72304

Author Manuscript Author Manuscript Author Manuscript Author Manuscript

REAGENT or RESOURCE	SOURCE	IDENTIFIER
Dispase (100mL)	Stem Cell Technologies	Cat# 07913
Accutase (100mL)	Stem Cell Technologies	Cat# AT104
LDN-193189	Sigma	Cat# SML0559
SB431542	Abcam	Cat# ab120163
XAV939	Sigma	Cat# X3004
Purmorphamine	Stem Cell Biotech	Cat# 72204
Puromycin	Sigma	Cat# P8833
BDNF	Prepotech	Cat# 450–02
Ascorbic acid	Sigma	Cat# A92902
O.C.T compound	Tissue-Tek	Cat# 4583
Bovine serum albumin	American Bioanalytical	Cat# AB01088
ProLong Gold Antifade Reagent	ThermoFisher	Cat# P36930
Critical commercial assays		
Papain Dissociation System	Worthington Biochemical Corporation	Cat# LK003150
Human Stem Cell Nucleofector Kit 1	Lonza	Cat# VPH-5012
RNeasy mini kit	QIAGEN	Cat# 74104
RNase-Free DNase Set	QIAGEN	Cat# 79254
iScript cDNA synthesis kit	Biorad	Cat# 1708891
SsoFast EvaGreen Supermix	Biorad	Cat# 1725201
Deposited data		
Raw and proposed scRNA-seq	This paper	GSE302899
scRNA-seq for human fetal and adult brains	Darmanis et al. [23]	SRA: SRP057196
Genes for neurological diseases	Pinero et al.[24]	https://www.disgenet.org/
Experimental models: Cell lines		
HES-3 NKX2–1$^{GFP/w}$	Elefanty lab	https://www.ncbi.nlm.nih.gov/pubmed/21425409
HES-3 NKX2–1$^{GFP/w}$;AAVS1-CAG-mCherry	This paper	N/A
Recombinant DNA		

Author Manuscript Author Manuscript Author Manuscript Author Manuscript

REAGENT or RESOURCE	SOURCE	IDENTIFIER
AAVS1-TALEN-L	Addgene	59025
AAVS1-TALEN-R	Addgene	59026
Oligonucleotides		
See Table S1 for oligonucleotides used in this paper	This paper	N/A
Other		
U-bottom ultra-low-attachment 96-well plate	Corning	CLS7007–24EA
Ultra-low-attachment 6-well plate	Corning	CLS3471–24EA
Ultra-low-attachment 24-well plate	Corning	3473
35 mm dish (with glass bottom)	MatTek	P35GC-0–10-C
Orbital shaker	IKA	KS260
Nucleofector	Lonza	AAB-1001
Software and algorithms		
Fiji	Schindelin et al. [54]	https://imagej.net/
CellRanger (v3.0.2)	10x Genomics	https://support.10xgenomics.com/single-cell-gene-expression/software/downloads/latest
Seurat (v3.0.2)	Ravin et al. [55]	https://github.com/satijalab/seurat/releases/tag/v3.0.0
GOstats (v2.46.0)	Falcon and Gentleman [56]	https://www.bioconductor.org/packages/release/bioc/html/GOstats.html
Bioconductor (v3.8)	N/A	https://www.bioconductor.org/
R (v3.5.0)	N/A	https://www.r-project.org/
GSEAPY (v0.9.3)	N/A	https://pypi.org/project/gseapy/
GSEA (v2.2.2)	Subramanian et al.[57]	https://www.gsea-msigdb.org/gsea/index.jsp
Tophat2 (v2.2.1)	Trapnell et al.[58]	https://support.10x.genomics.com/single-cell-gene-expression/software/downloads/latest
Cufflinks (v1.2.0)	Trapnell et al.[59]	http://cole-trapnell-lab.github.io/cufflinks/